molecules

MDPI

Article

Synthesis, Characterization, and In Vivo Anti-Cancer Activity of New Metal Complexes Derived from Isatin-*N*(4)antipyrinethiosemicarbazone Ligand Against Ehrlich Ascites Carcinoma Cells

Fathy El-Saied [1], Bishoy El-Aarag [2,3,*], Tarek Salem [4], Ghada Said [1], Shaden A. M. Khalifa [5,6] and Hesham R. El-Seedi [1,7,8,9,*]

1 Department of Chemistry, Faculty of Science, Menoufia University, Shebin El-Koom 32512, Egypt; elsayedfathy139@yahoo.com (F.E.-S.); ghadasaid_2007@yahoo.com (G.S.)
2 Biochemistry Division, Chemistry Department, Faculty of Science, Menoufia University, Shebin El-Koom 32512, Egypt
3 Division of Chemistry and Biotechnology, Graduate School of Natural Science and Technology, Okayama University, Okayama 7008530, Japan
4 Department of Molecular Biology, Genetic Engineering & Biotechnology Institute, University of Sadat City, Sadat City 32958, Egypt; salem_tarek@yahoo.com
5 Department of Molecular Biosciences, The Wenner-Gren Institute, Stockholm University, SE 106 91 Stockholm, Sweden; shaden.khalifa@su.se
6 Department of Experimental Cancer Medicine (ECM); Novum, 14157 Huddinge, Stockholm, Sweden
7 Pharmacognosy Group, Department of Medicinal Chemistry, Uppsala University, Biomedical Centre, Box 574, SE-751 23 Uppsala, Sweden
8 International Research Center for Food Nutrition and Safety, Jiangsu University, Zhenjiang 212013, China
9 Al-Rayan Research and Innovation Center, Al-Rayan Colleges, Medina 42541, Saudi Arabia
* Correspondence: bishoy.yousef@gmail.com (B.E.-A.); hesham.el-seedi@ilk.uu.se (H.R.E.-S.); Tel.: +20-1271732703 (B.E.-A.); +46-700434343 (H.R.E.-S.)

Received: 18 July 2019; Accepted: 9 September 2019; Published: 11 September 2019

Abstract: The current study aimed to synthesize new metal coordination complexes with potential biomedical applications. Metal complexes were prepared via the reaction of isatin-*N*(4)antipyrinethiosemicarbazone ligand **1** with Cu(II), Ni(II), Co(II), Zn(II), and Fe(III) ions. The obtained metal complexes **2**–**12** were characterized using elemental, spectral (^{1}H-NMR, EPR, Mass, IR, UV-Vis) and thermal (TGA) techniques, as well as magnetic moment and molar conductance measurements. In addition, their geometries were studied using EPR and UV–Vis spectroscopy. To evaluate the in vivo anti-cancer activities of these complexes, the ligand **1** and its metal complexes **2**, **7** and **9** were tested against solid tumors. The solid tumors were induced by subcutaneous (SC) injection of Ehrlich ascites carcinoma (EAC) cells in mice. The impact of the selected complexes on the reduction of tumor volume was determined. Also, the expression levels of vascular endothelial growth factor (VEGF) and cysteine aspartyl-specific protease-7 (caspase-7) in tumor and liver tissues of mice bearing EAC tumor were determined. Moreover, their effects on alanine transaminase (ALT), aspartate transaminase (AST), albumin, and glucose levels were measured. The results revealed that the tested compounds, especially complex **9**, reduced tumor volume, inhibited the expression of VEGF, and induced the expression of caspase-7. Additionally, they restored the levels of ALT, AST, albumin, and glucose close to their normal levels. Taken together, our newly synthesized metal complexes are promising anti-cancer agents against solid tumors induced by EAC cells as supported by the inhibition of VEGF and induction of caspase-7.

Keywords: metal complexes; isatin-*N*(4)antipyrinethiosemicarbazone; Ehrlich ascites carcinoma; tumor volume; VEGF; caspase-7

1. Introduction

Cancer is considered one of the most devastating life-threatening disease worldwide. It is characterized by uncontrolled cell growth and the rapid spread of abnormal cells [1]. Angiogenesis is a vital regulator of tumor growth, spread and metastasis [2]. Tumor angiogenesis, which is the development of new blood vessels, is regulated by the production of angiogenic stimulators such as vascular endothelial growth factor (VEGF). VEGF is a key regulatory factor in the prognosis of various cancers; therefore, the inhibition of VEGF production is an alternative therapeutic approach for cancer treatment [3–6].

Chemotherapy, along with surgery, radiation, hormone therapy, and immune therapy, is used to treat cancer [7]. Despite the success of controlling the tumor growth in several cases, the incidence and prevelance of cancer is still dramtically increasing and calling for new chemotherapeutics to be introduced to the pharmaceutical industry and the market [8]. Antipyrine (2,3-dimethyl-1-phenyl-5-pyrazolone) and its derivatives possess a diverse array of potentially useful biological properties [9]. Similarly, thiosemicarbazones have demonstrated significant biological applications, as antitumor [10], antifungal [11], antiviral [12], antibacterial [13] and antimalarial [14] agents. Previous investigations involving the synthesis, characterization and biological evaluation of iron(III), cobalt(II), cobalt(III), nickel(II), zinc(II), and copper(II) complexes of 4-formylantipyrine *N*(4)-substituted thiosemicarbazones have been reported [15,16].

Based on these results and as a continuation of our ongoing interest in compounds with antitumor activities, the present study was carried out to synthesize and characterize metal complexes of isatin-*N*(4)antipyrinethiosemicarbazone and to evaluate their anti-tumor, anti-angiogenic and apoptotic activities against solid tumors induced by Ehrlich ascites carcinoma (EAC) cells in mice.

2. Results and Discussion

All the prepared metal complexes, shown in Figure 1, are stable at room temperature, non-hygroscopic and insoluble in most organic solvents and water, but they are completely soluble in dimethylformamide (DMF) and dimethylsulfoxide (DMSO). The elemental analyses, physical data, are listed in Table 1. The elemental analyses confirmed that complexes **2**–**6**, **8** and **10** are formed in a 1:1 molar ratio of the metal ion and ligand, whereas complexes **9**, **11** and **12** are formed in a 1:2 molar ratio of the metal ion and the ligand. Complex **7** is a binuclear complex.

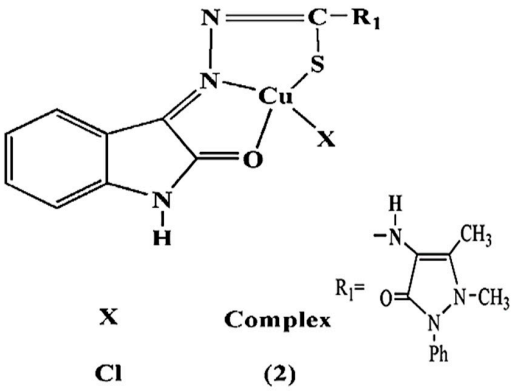

X	Complex
Cl	(2)
Br	(3)
NO_3	(4)
OAc	(5)
ClO_4	(6)

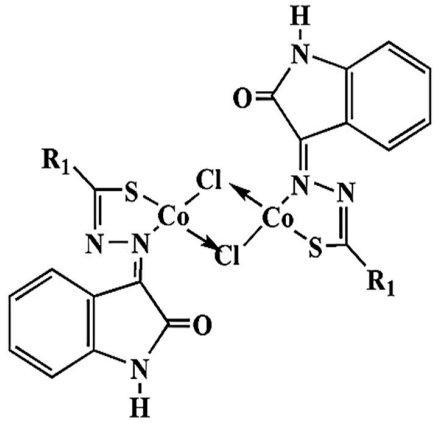

Complex 7

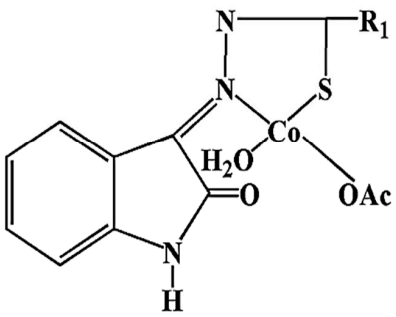

Complex 8

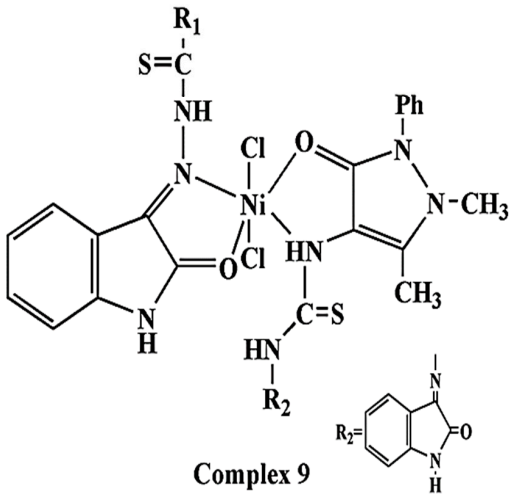

Complex 9

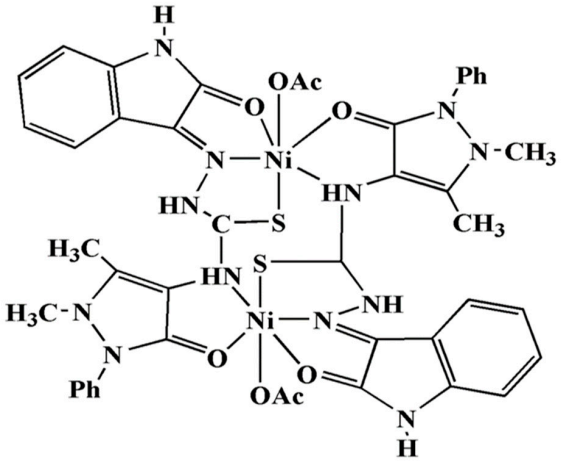

Complex 10

Figure 1. *Cont.*

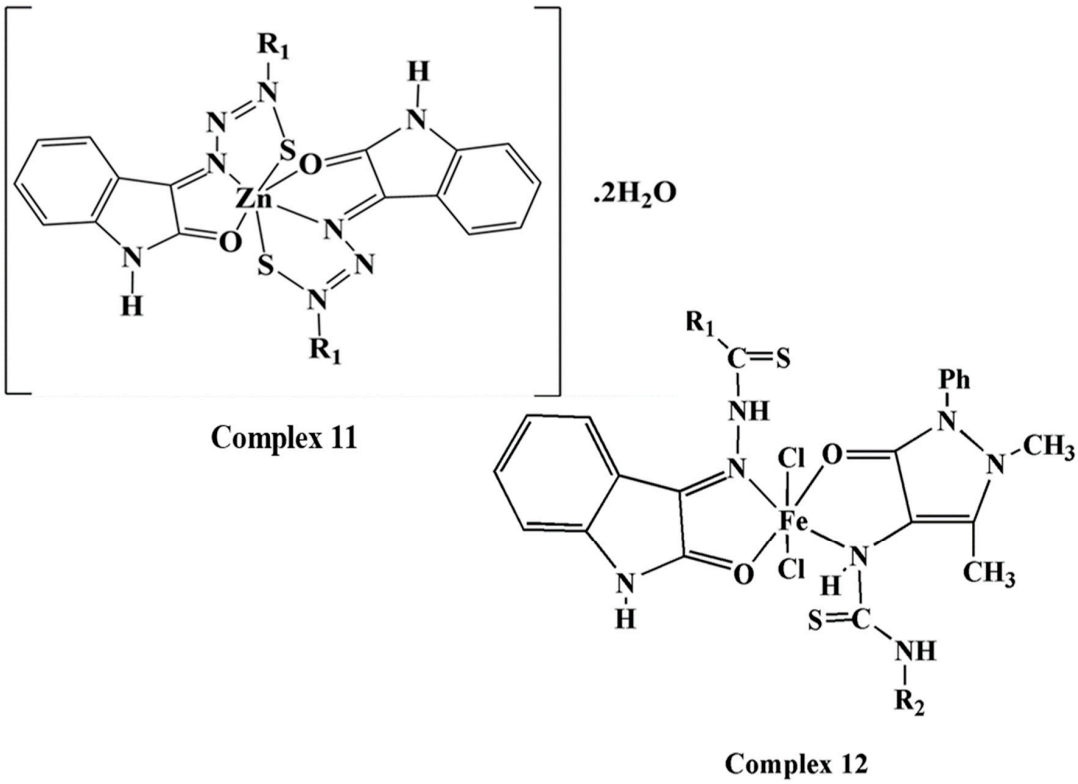

Figure 1. Chemical structures of metal complexes **2–12**.

Table 1. Analytical and physical data of the ligand **1** and its metal complexes **2–11**.

No.	Molar Ratio/Compound	Color	m.p. (°C)	F.W.	Yield%	Analysis (%)/Found (Calcd)				Molar Conductance
						C	H	N	S	
1	HL $C_{20}H_{18}N_6O_2S$	Yellow	210–212	406.64	94	59.14(59)	5.15(4.43)	20.91(20.66)	7.85(7.87)	-
2	HL+$CuCl_2$(1:1),(2:1),(1:2) [CuLCl]·H_2O	Deep brown	238–240	522.6	79	46.0(46)	4.1(3.64)	16.3(16.10)	6.88(6.13)	10.0
3	HL+$CuBr_2$(1:1) [CuLBr]·$3H_2O$	Brown	250	602.5	89	38.81(39.83)	3.54(3.82)	15.02(13.94)	5.03(5.31)	37.9
4	HL+$Cu(NO_3)_2$·$3H_2O$ (1:1)[$Cu(NO_3)$ L]·H_2O	Brown	247	548.5	80	43.4(43.5)	3.29(3.5)	18(17.9)	6(5.8)	34.3
5	HL+$Cu(OAc)_2$ (1:1) [Cu(OAc) L]·$2H_2O$	Brown	212–216	563.5	74	46.12(46.90)	4.82(4.30)	15.13 (14.9)	5.1(5.7)	11.9
6	HL+$Cu(ClO_4)_2$(1:1) [$Cu(ClO_4)$L]·$2H_2O$	Brown	250–252	604.5	91	38.92(39.7)	3.75(3.48)	14.67(13.91)	5.18(5.29)	70.32
7	HL+$CoCl_2$ (1:1) [CoClL]$_2$·$2H_2O$	Brown	258-260	1036	66	47(46.33)	4.17(3.7)	17(16.21)	6.4(6.18)	47.9
8	HL+$Co(OAc)_2$ (1:1) [Co(OAc) L(H_2O)]·$4H_2O$	Brown	Over 300	614.5	75	42.96(41.9)	5.3(5.04)	14.2(13.7)	4.87(5.2)	4.6
9	Hl+$NiCl_2$ (1:1) [$NiCl_2$(HL)$_2$]·$4H_2O$	Brown	254–255	1014.9	84	46.84(47.3)	4.94(4.33)	16.95(16.55)	5.89(6.3)	13.5
10	HL+$Ni(OAc)_2$ (1:1) [Ni(OAc) L]·$2H_2O$	Brown	Over 300	558.9	70	47.76(47.24)	4.19(4.3)	15. 6(15.03)	6.71(5.78)	2.6
11	HL+$Zn(OAc)_2$ (1:1) [ZnL_2·H_2O	Deep yellow	Over 300	912.2	69	51.9(52.6)	3.7(4.2)	18.8 (18.42)	6.64 (7)	1.4
12	HL+$FeCl_3$ (1:1) [$FeCl_2$(HL)$_2$]Cl·H_2O	Deep green	210–212	993.7	78	47.62(48.3)	3.9(3.8)	16.95(16.91)	5.6(6.44)	54.09

2.1. ^{1}H-NMR Spectra

The ^{1}H-NMR spectra of the ligand **1** and the zinc complex **11** are illustrated in the Supplementary Materials. The data shows three separate singlets at 12.819, 11.219 and 10.115 ppm, which can be attributed to the thiosemicarbazide N-N(2)H, the indole N-H moiety and the thiosemicabazide CS-N(4)-H, respectively [17]. Multiple signals appear in the 7.702–6.876 ppm region, and these can be attributed to the aromatic protons of the indole and phenyl rings of antipyrine. The other signals for the ligand at 3.068 (s, 3H) and 2.135 (s, 3H) correspond to the N-CH_3 and C-CH_3 of the antipyrine moiety, respectively [15]. The ^{1}H-NMR spectrum of complex **11** does not show a signal corresponding to N-N(2)H of thiosemicarbazide, suggesting the loss of the thiol proton, and the binding ligand in its thiol form. The spectrum displays signals attributable to the indole N-H moiety, the CS-N(4)-H of thiosemicabazide and all the other characteristic signals at the same positions as those of the free ligand.

2.2. Mass Spectra

The mass spectra of ligand **1** and complexes **7**, **8**, **11**, and **12** are shown in the Supplementary Materials. The molecular ion peak at *m*/*z* 406.27 amu in the spectrum of the ligand **1** is consistent with the molecular weight of its proposed structure. Moreover, the fragmentation pattern shows ion peaks at *m*/*z* 363.47, 291.15, 276.68, 261.69, 223.71, 204.07, 203.30, 145.64, 130.57, 118.18 and 76.3 amu corresponding to $C_{19}H_{17}N_5OS$, $C_{13}H_{17}N_5OS$, $C_{12}H_{13}N_5OS$, $C_{12}H_{13}N_4OS$, $C_9H_{10}N_4OS$, $C_9H_6N_3OS$, $C_{11}H_{13}N_3O$, $C_8H_5N_2O$, C_8H_5NO, C_7H_5NO and C_6H_5 fragments, respectively.

The mas spectrum of complex **7** (F.W. = $C_{40}H_{38}N_{12}O_6S_2Co_2Cl_2$) shows a molecular ion peak at *m*/*z* 999.5 amu, consistent with a molecular weight of 998.8 g/mol, which is the molecular weight of the complex after the loss of one molecule of hydration water (F.W. = $C_{40}H_{34}N_{12}O_4S_2Co_2Cl_2$). The spectrophotometer at hand cannot detect molecular ions with molecular weights greater than 1000 g/mol. The fragment ion peaks at *m*/*z* 868.9 and 463.9 amu correspond to the formulas $C_{40}H_{34}N_{12}O_4S_2Co$ and $C_{20}H_{17}N_6O_2Co$.

The mass spectrum of complex **8** ($C_{22}H_{30}N_6O_9SCo$, F.W. = 612.5) displays a molecular ion peak at *m*/*z* 612.85 (100%) amu, confirming the suggested structure of the complex. Moreover, the spectrum shows several peaks, including peaks at *m*/*z* 576.23 (94.07), 561.30 (61.93), 541.85 (6.86), and 523.22 (39.20), corresponding to the formula $C_{22}H_{26}N_6O_7SCo$, $C_{22}H_{24}N_6O_6SCo$, $C_{22}H_{22}N_6O_5SCo$, and $C_{22}H_{20}N_6O_4SCo$, respectively, due to the sequential loss of two molecules of water of hydration, another water of hydration, a final water of hydration, and one coordinated water molecule, respectively.

The mass spectrum of complex **11** ($C_{40}H_{38}N_{12}O_6S_2Zn$, F.W. = 911.50) displays a molecular ion peak at *m*/*z* 911.95 (1.19), consistent with the suggested structure.The mass spectrum of complex **12** ($C_{40}H_{38}N_{12}O_5S_2FeCl_3$, F.W. = 992.50) exhibits a molecular ion peak at *m*/*z* 992.50 amu, confirming the putative molecular weight of the complex. Moreover, the spectrum shows several ion peaks, including peaks at 973.50 (1.90), 938.30 (12.96), 869.80 (8.27), and 464.40 (2.48) corresponding to the formula $C_{40}H_{36}N_{12}O_4S_2FeCl_3$, $C_{40}H_{38}N_{12}O_5S_2FeCl_3$, $C_{40}H_{38}N_{12}O_5S_2FeCl_2$, $C_{40}H_{38}N_{12}O_5S_2Fe$ and $C_{20}H_{18}N_6O_2SFe$, which are attributable to the losses of one water of hydration, an ionisable chloride, two coordinated chloro ligands and one ligand, respectively.

2.3. The Molar Conductance

The molar conductance values of the metal complexes in DMF (10^{-3} M) were illustrated in Table 1. The results showed that none of the complexes except **12** are electrolytes [16], indicating that the anions in all these complexes are directly bound to the metal ion. Complex **12** gave a molar conductance of 74.5 $\Omega^{-1}cm^2mol^{-1}$ attributable to a 1:1 electrolyte, and indicating the presence of a chloride ion in the outer coordination sphere [18]. The high value of molar conductance of complex **6** may be associated with the partial displacement of the perchlorato ligand by DMF [15].

2.4. Infrared (IR) Spectra

The IR spectra of the ligand **1** and its metal complexes **2–12** were shown in Supplementary Materials. The most diagnostic infrared spectral bands are illustrated in Table 2; the infrared spectrum of the ligand **1** displays bands at 3442, 3348, 3287, 3251, and 3141 attributable to ν(N-H) absorptions characteristic of –NH groups [19,20]. The spectrum also displays bands at 1738, 1645, 1688, 1623 and 1595 cm^{-1}. The first band can be assigned to ν(C=O) of the isatin moiety [19,20], and the second band can be assigned to ν(C=O) of the antipyrine moiety. The latter three bands are associated with ν(C=N) [21]. The appearance of multiple bands characteristic of ν(C=N) can be explained by the formation of tautomers secondary to the presence of the isatin carbonyl group and C=S with the adjacent –NH groups. The absorption band of ν(C=S) (thioamide IV) observed at 881 cm^{-1} [15] and a weak band observed at 2650 cm^{-1}, assigned to ν(C-SH), supported the thione-thiol tautomerization expected from the C=S group with an adjacent proton [22].

The binding mode of the ligand in each metal complex has been deduced by comparing the IR spectrum of the ligand with that of the corresponding metal complex. In the infrared spectra of all the complexes, the band characteristic of the ν(C=N) of the isatin moiety is shifted to lower wave numbers compared to that of the free ligand, indicating the coordination of C=N group with the metal via the nitrogen atom in all complexes. In the IR spectra of the metal complexes, except for those of **7** and **8**, the bands corresponding to the C=O of the isatin moiety appeared at lower wavenumbers compared to that of the ligand as a result of the participation of the carbonyl oxygen atom of this group in the coordination. This band did not shift in the infrared spectra of complexes **7** and **8**, indicating that C=O is not involved in the coordination.

In the infrared spectra of the complexes, except **9**, **10** and **12**, the absorption band is attributable to the ν(C=O) of the antipyrine moiety appeared at the same position as that of the ligand, indicating that this group only participates in coordination to the metal ion in complexes **9**, **10** and **12**. In the infrared spectra of all complexes, except **9** and **12**, the band corresponding to ν(C=S) appeared at lower wavenumbers (808–848 cm^{-1}) compared to that of the free ligand, indicating that the C-S group takes part in the coordination. The appearance of a band at 1622–1560 cm^{-1}, which is assignable to υ(–N=C-S-), accompanies the shift in the ν(C-S) band. The appearance of the later band indicates the participation of the thiol form in coordination rather than the thion form, as suggested by the ^{1}H-NMR spectrum of complex **11**. The ν(C=S) bands in the infrared spectra of complexes **9** and **12** were at the same position as that of the free ligand, indicating that the C=S moiety does not participate in coordination in complexes **9** and **12**.

Complexes **9** and **12** are composed of two ligand molecules that bind to one metal ion, and their infrared spectra showed that the two ligand molecules have different binding modes. In the infrared spectra of the complexes **9** and **12**, each exhibits four bands at 1735–1737, 1700–1660, 1645 and 1620 cm^{-1}, attributable to the uncoordinated ν(C=O) of the isatin moiety, the coordinated ν(C=O) of the isatin moiety, the uncoordinated ν(C=O) of the antipyrine moiety and the coordinated ν(C=O) of the antipyrine moiety, respectively. Moreover, each of the spectra of complexes **9** and **12** displays two bands corresponding to the ν(C=N) of the isatin moiety at 1595 and 1520 cm^{-1}, which are assignable to the free uncoordinated C=N and the coordinated C=N, respectively. The above results illustrate that one of the ligand molecules behaves as a neutral, bidentate ligand and coordinates via the C=N and C=O groups of the isatin moiety and that the second molecule also behaves as a neutral, bidentate ligand but coordinates via the C=O and N-H groups of the antipyrine moiety.

The spectra of acetato complexes **5**, **8** and **10** show two absorption bands at 1620–1615 and 1372–1333 cm^{-1}, assigned to υ(C=O) and υ(C-O), respectively. The difference between these two bands is approximately 287–243 cm^{-1}, which indicates that the acetate in these complexes coordinates to the metal ion as a monodentate ligand [23]. The monodentate coordination of a perchlorate ligand lowers the symmetry of the system ($T_d \rightarrow C_{3v}$). The modes of the free perchlorate that were initially degenerated (υ_3 and υ_4) are both split into two bands [24]. The infrared spectrum of the perchlorate $[Cu(ClO_4)L]\cdot 2H_2O$ complex showed that both the υ_3 band and υ_4 band are split into two bands, at 1118

and 1085 cm^{-1} and at 694 and 631 cm^{-1}, respectively, indicating that the perchlorate coordinates to the metal ion as a monodentate ligand. The infrared spectrum of complex **4**, $[Cu(NO_3)L]\cdot H_2O$ showed two bands at 1462 and 1382 cm^{-1}, attributable to a monodentate nitrato ligand [25]. The infrared spectra of the hydrated complexes display a broad band at 3491–3388 cm^{-1} from ν(OH) of the water molecule [26]. The IR spectra of all the complexes display a new band at 591–498 cm^{-1}, assigned to ν(M-N) [27–29], and the spectra of all the metal complexes except **7** and **8** show a new band at 693–589 cm^{-1}, assigned to υ(M-O) [19–29].

Table 2. IR spectral bands (cm^{-1}) for ligand **1** and its metal complexes **2–12** and their assignments.

No.	Ligand/Complexes	ν(H_2O)	ν(N^4H)	ν(C=O)	ν(C=N)	ν(C=S)	ν(M-O)	ν(M-N)	ν($OAc/ClO_4/NO_3$
1	Ligand $C_{20}H_{18}N_6O_2S$	-	3442, 3348, 3287, 3251, 3141	1738 [a], 1645 [b]	1688 [a], 1623, 1595	881	-	-	-
2	$[CuClL]\cdot 2H_2O]$	3395	3161, 3100	1702 [a], 1645 [b]	1616, 1539	808	632	498	-
3	$[CuBrL]\cdot 3H_2O$	3446	3106	1695 [a], 1643(sh) [b]	1622, 1578	-	614	504	-
4	$[Cu\ (NO_3)\ L]\cdot H_2O$	3425	3166	1703 [a], 1645 [b]	1620, 1539	808	638	586	1382–1462
5	$[Cu(OAc)L]\cdot 2H_2O$	3417	3237	1680 [a], 1645 [b]	1560, 1525	847	595	503	1615, 1333
6	$[Cu(ClO_4)L]\cdot 2H_2O$	3428	3325, 3170	1628 [a], 1645 [b]	1568, 1516	838	631	505	1085, 1049
7	$[CoClL]_2\cdot 2H_2O$	3388	3150	1734 [a], 1645 [b]	1600, 1515	840	629	585	-
8	$[Co\ (OAc)\ L(H_2O)]\cdot 4H_2O$	3491, 3422	3196	1734 [a], 1645 [b]	1590, 1545	841	630	540	1619, 1372
9	$[NiCl_2(HL)_2]\cdot 4H_2O$	3441	3280	1735 [a], 1660 [a], 1645 [b]. 1610 [b]	1688, 1620	877	648	591	-
10	$[Ni(OAc)\ L]\cdot 2H_2O$	3445	3310, 3200	1664 [a] (sh), 1640 [b]	1580, 1540	829	590	503	1620, 1342
11	$[Zn\ L_2]\cdot 2H_2O$	3413	3223	1700 [a], 1643 [b]	1609	848	612	580	-
12	$[FeCl_2(HL)_2]Cl\cdot H_2O$	3429(s,br)	3280	1737 [a], 1700 [a], 1645 [b], 1610 [a]	1685, 1620	881	589	512	-

[a] indigo moiety, [b] antipyrine moeity, -: indicates no value available.

2.5. Magnetic and Electronic Spectra

The room-temperature magnetic moments (μ_{eff} BM per metal atom) and electronic spectral bands for the metal complexes in the solid state are described in Table 3. The data showed that the electronic absorption spectrum of ligand **1** exhibits bands at 268 and 280 nm, attributable to intra-ligand $\pi \rightarrow \pi^*$ electronic transitions [15,30]. These bands do not change significantly upon complex formation [31].

The somewhat broad band at 369 nm is assignable to the intra-ligand $n \rightarrow \pi^*$ electronic transitions associated with the combination of the azomethine function of the thiosemicabazone, the thione function of the thiosemicabazone and the heterocyclic moiety [15,32]. In the spectra of the metal complexes, this band generally shifts to a higher energy as a result of the participation of the azomethine and/or thiol groups in coordination [33,34]. In the spectra of the metal complexes, new bands were observed in the 357–530 nm region due to S(π)→metal(II,III) charge-transfer processes [35,36], and the spectrum of bromo complex **3** showed a Br→metal(II) charge-transfer band [37]. Cl→metal(II,III) [38–40] and O→metal(II,III) [35] charge-transfer bands were generally observed at approximately 333 nm and were obscured by the stronger intra-ligand transfer bands. Copper(II) complexes **2**–**6** showed magnetic moments of 1.76–1.87 BM. These values are close to the spin-only value for one unpaired spin (~1.73 BM) and indicate that there is no molecular association between the copper(II) ions in the square planar environment [34,41,42]. The electronic absorption spectra of Cu(II) complexes **2**–**5** showed two or three bands at 870–660, 740–631 and 675–580 nm, assignable to the $^2B_1g(d_{x2-y2}) \rightarrow {}^2A_{1g}(d_{z2})$, $^2B_1g(d_{x2-y2}) \rightarrow {}^2B_{2g}(d_{xy})$ (υ_2) and $^2B_1g(d_{x2-y2}) \rightarrow {}^2Eg(d_{xz},d_{yz})$ (υ_3) transitions, suggesting a square planar geometry around the copper(II) ion. Complex **6** displays a broad band at 790 nm that could be attributed to the abovementioned transitions in the ligands in a square planar geometry around the copper(II) ion [43–45].

Cobalt(II) complex **7** gave a magnetic moment of 3.1 BM, which is considerably less than what is expected for high-spin tetrahedral cobalt(II). This unexpected value could be explained by the occurrence of antiferromagnetic exchange through the chloro bridge linking the two cobalt(II) ions [46,47]. Complex **8** gave a magnetic moment of 3.7 BM per metal ion, which is consistent with high-spin tetrahedral cobalt(II) complexes [48]. The electronic spectra of complexes **7** and **8** displayed a broad band with several features at approximately 675 nm, which is attributable to the $^4A_2 \rightarrow {}^4T_1(P)$ (υ_3) transition in a tetrahedral geometry around the Co(II) ion [15].

The nickel(II) complexes were found to be paramagnetic, which ruled out square planar configurations. The magnetic moments of nickel(II) complexes **9** and **10** are 2.98 and 3.06 BM, respectively, corresponding to two unpaired electrons [49], suggesting geometries other than square planar. The electronic spectra of Ni(II) complexes **9** and **10** showed bands at 950, 690-675 nm and 560−567 nm, assignable to the $^3A_{2g}(\mathbf{F}) \rightarrow {}^3T_{2g}(\mathbf{F})(\upsilon_1)$, $^3A_{2g}(\mathbf{F}) \rightarrow {}^3T_{1g}(\mathbf{F})(\upsilon_2)$ and $^3A_{2g}(\mathbf{F}) \rightarrow {}^3T_{1g}(\mathbf{P})$ transitions, respectively, in an octahedral environment [50–52]. The υ_2/υ_1 ratios for these complexes are 1.41 and 1.37, which are below the usual range of 1.5–1.75. These ratios suggest a tetragonally distorted octahedral geometry around the nickel(II) ions [51,53].

Iron(III) complex **12** gave a magnetic moment of 5.95 BM per metal ion, corresponding to a high-spin d^5 configuration. The electronic spectrum of complex **12** showed strong bands at 391, 450, 530 and 584 nm. The first three bands can be assigned to ligand-to-metal charge-transfer (LMCT) processes. The last band at 584 nm is broad and of relatively high intensity. The relatively high intensity of this band can be attributed to overlap with a low-lying ligand charge-transfer band. This is because in the case of iron(III), the d-d transitions are considered forbidden because they take place between ions with different multiplicities; examples of such transitions include the $^6A_1g \rightarrow {}^4T_{1g}$ (G), $^6A_1g \rightarrow {}^4T_{2g}$ (G) and $^6A_1g \rightarrow {}^4E_g$ (G) or ^4E_g(D) transitions in tetragonally distorted octahedral Fe(III) environments [54]. The electronic spectrum of the zinc(II) complex showed bands at 396, 440, 491, and 520(sh), which can be attributed to ligand-to-metal (L→M) charge-transfer processes.

Table 3. The electronic absorption spectral bands (nm) and magnetic moments of ligand **1** and its metal complexes **2**–**12**.

No.	Compound	π→π* (nm)	n→π*	Charge Transfer	d→d Bands	μ_{eff} (β.M)
1	HL $C_{20}H_{18}N_6O_2S$	268	280, 369			-
2	$[CuLCl]\cdot 2H_2O$	291	310, 395		600, 672, 770	1.03
3	$[CuLBr]\cdot 3H_2O$	295	325, 445		580, 631	1.1
4	$[Cu(NO_3)\ L]\cdot H_2O$	270	310, 455	520, 574	675, 720	1
5	$[Cu(OAc)\ L]\cdot 2H_2O$	270	310		560, 671	1.11
6	$[Cu(ClO_4)L]\cdot 2H_2O$	270	363, 400		500(br), 770(br)	1.6
7	$[CoClL]_2\cdot 2H_2O$	260	318, 345		600, 675, 700	0.42
8	$[Co(OAc)\ L(H_2O)]\cdot 4H_2O$	290	320		600, 675, 780	3.7
9	$[NiCl_2(HL)_2]\cdot 4H_2O$	290	310, 396	420	500	-
10	$[Ni\ (OAc)\ L]\cdot 2H_2O$	291	305		567, 950	2.26
11	$[ZnL_2]\cdot 2H_2O$	280	319, 396	480, 520(sh)	-	-
12	$[FeCl_2(HL)_2]Cl\cdot H_2O$	270	300, 391	450	584	4.67

-: indicates no value available.

2.6. EPR Spectra of the Copper(II) Complexes

The EPR spectra of the Cu(II) complexes are illustrated in the Supplementary Materials. The EPR data of Cu(II) complexes **2**–**6** in the polycrystalline state at 298 K are listed in Table 4. The EPR spectra of the Cu(II) complexes have low g_1 and g_{av} values, indicating that the bonds have considerable covalent characteristics [18,55]. The EPR spectra of the Cu(II) complexes other than complex **5** ($[Cu(L)(OAc)]\cdot 2H_2O$) show rhombic-type distortion with three g values, g_1 = 2.189, 2.198, 2.287, and 2.25; g_2 = 2.121, 2.079, 2.121, and 2.12; and g_3 = 2.057, 1.989, 1.977, and 2.027, respectively. The rhombic symmetry of these complexes is attributable to the bulkiness of the ligand and to the unequal bond lengths of the four Cu-S, Cu-N, Cu-O, and Cu-X bonds (X=Cl, Br, NO_3 or ClO_4) [55]. The g tensors, which follow $g_1 > g_2 > g_3 > 2$, are indicative of complexes with a $d_{(x2-y2)}$ ground state. This result is supported by the value of R ($R = (g_2 - g_1/(g_3 - g_2) < 1 (= 0.94 - 0.72)$), confirming a $d_{(x2-y2)}$ ground state with covalent bonding character [56,57].

The EPR spectral data of complex **5** demonstrate anisotropic signals with $g_{\|} > g_{\perp} > 2.0023$, which are indicative of a $d_{(x2-y2)}$ ground state with axial symmetry, resulting in a $^2B_{1g}$ ground state that is known for Cu^{2+} complexes [58,59]. These g values are consistent with Cu^{2+}-complex **5** having a square planar geometry [60,61]. The geometric parameter G, which is a measure of the exchange interaction between the copper centres in the solid state, was calculated using the equation $G = (g_{\|} - 2.0023)/(g_{\perp} - 2.0023)$ for axial and rhombic compounds, $g_{\|} = g_1$ and $g_{\perp} = g_2 + g_3/2$. If G > 4, the exchange interaction is negligible, and if it is less than 4, considerable exchange interactions exist [58,62]. Complexes **3**, **4**, and **5** have G values > 4, indicating that exchange interactions are negligible, while for complexes **2** and **6**, G < 4, suggesting considerable exchange interactions between the Cu(II) centres. Kivelson and Neiman reported that the $g_{\|}$-values of Cu^{2+} complexes can be used to determine the nature of the copper-ligand bonding. If the $g_{\|}$-value is smaller than 2.3, the environment is essentially covalent, while if the value is larger than 2.3, the environment is essentially ionic [63]. For all the synthesized complexes, $g_{\|} < 2.3$, indicating that there is considerable covalent character in the copper-ligand bonds.

According to [45,64,65], the orbital reduction factor (k) and its parallel ($k_{\|}$) and perpendicular ($k_{\perp}$) components were calculated according to the following equations: $k_{\|}^2 = (g_{\|} - 2.0023)\Delta_2/8\lambda_0$, $k_{\perp}^2 = (g_{\perp} - 2.0023)\ \Delta_1/2\ \lambda_0$, $k^2 = (K_{\|}^2 + 2_{\perp}^2)/3$ where λ_o is the spin orbit coupling ($-828\ cm^{-1}$) of the free Cu(II) ion, and Δ_1 and Δ_2 are the electronic transitions $^2B_{1g} \rightarrow {}^2B_{2g}$ ($d_{x2-y2} \rightarrow d_{xy}$) and $^2B_{1g} \rightarrow {}^2E_g$ ($d_{x2-y2} \rightarrow d_{xz}d_{yz}$),

respectively. The calculated $k_{\|}^2$, $k_{\perp}^2$ and k^2 values in Table 1 showed that for complexes 3–6, $k_{\|} > k_{\perp}$, indicating the presence of significant out-of-plane π-bonding [66] and confirming that $^2B_{1g}$ is the ground state for these complexes. For complex 2, $k_{\|} < k_{\perp}$, indicating the presence of significant in-plane π-bonding [67]. Moreover, when the environment is ionic, k = 1, but if this value is less than 1, the environment is covalent. These compounds showed k values lower than one, which is strong evidence of covalent character, which is in agreement with the results obtained from the $g_{\|}$ values [65,68]. None of the solid-state EPR spectra of the complexes displayed hyperfine structure, confirming the presence of intermolecular interactions, but these interactions were not strong enough to overcome the dipolar interactions [69].

Table 4. EPR spectral assignments and bonding parameters for Cu(II) complexes in polycrystalline state at 298 K.

Parameter	Complex 2	Complex 3	Complex 4	Complex 5	Complex 6
$g_{\|}$ or g_1	2.189	2.198	2.287	$g_{\|}$ = 2.21	2.25
$g_{\perp}$ or g_2, g_3	2.121, 2.057	2.079, 1.989	2.121, 1.977	$g_{\perp}$ = 2.038	2.12, 2.027
$g_{\perp}$	2.089	2.034	2.049	2.038	2.074
g_{av}	2.12	2.125	2.128	2.095	2.132
G	2.12	5.82	5.86	5.53	3.38
R	0.94	0.76	0.87	-	0.72
$k_{\|}^2/k_{\|}$	0.419/0.647	0.468/0.684	0.637/0.798	0.424/0.651	0.554/0.744
$k_{\perp}^2/k_{\perp}$	0.722/0.850	0.29/0.539	0.391/0.625	0.248/0.498	0.137/0.370
K^2/k	0.621/0.788	0.349/0.591	0.473/0.688	0.307/0.554	0.276/0.525

-: indicates no value available.

2.7. Thermal Analysis

The TGA spectra of metal complexes are shown in the Supplementary Materials. The TGA results of solid complexes **2**, **3**, **5** and **7**–**12** are listed in Table 5. The results show an agreement with the formulae suggested by the analytical, spectral and magnetic data. A general decomposition pattern, in which the complexes decompose in two or three stages, was observed. The first stage is the loss of waters by hydration at 29–160 °C; the second stage of decomposition corresponds to the loss of coordinated water molecules at 80–175 °C; complex **8** showed a third decomposition stage that is a result of overlapping processes including the loss of Cl^-, Br^- or OAc^- anions; the loss the ligands to form metal oxides or metal sulfides mixed with carbon residues; and the oxidation of carbon to carbon dioxide leaving metal oxides or sulfides.

Table 5. Thermal (TGA) data for metal complexes **2**, **3**, **5**, and **7**–**12**.

No.	Complex	Temp. Range (°C)	Weight Loss Found (calc)%	Assignment	Residual's Formula
2	$[Cu(L)Cl]\cdot H_2O]$	30–120 213–898	4.10 (3.44) 83.90(84.30)	Loss of water of hydration ($1H_2O$) Continuous decomposition of complex	[Cu(L)Cl] CuO
3	$[Cu(L)Br]\cdot 3H_2O$	26–75 191–763	9.3(8.96) 79.54(80.6)	Loss of water of hydration ($3H_2O$) Continuous decomposition of complex	[Cu(L)Br] CuO
5	$[Cu(L)OAc]\cdot 2H_2O$	30–109 109–800	6.60(6.40) 81.55(82.40)	Loss of water of hydration ($2H_2O$) Continuous decomposition of complex	[Cu(L)OAc] CuO
7	$[Co(L)Cl]_2\cdot 2H_2O$	45–145 195–470 625–660	4.20(3.50) 69.23(70.30) 8.30(8.10)	Loss of water of hydration ($2H_2O$) Partial decomposition of complex oxidation of carbon to CO_2	$[Co(L)Cl]_2$ 2CoS + 7C 2CoS
8	$[Co(L)OAc(H_2O)]\cdot 4H_2O$	27–80 80–175 195–550 600–898	11.30(11.73) 3.63(2.93) 66.00(66.51) 3.12(3.91)	Loss of water of hydration ($4H_2O$) Loss of coordinated water ($1H_2O$) Continuous decomposition of complex to form metal oxide and carbon Partial oxidation of carbon	[Co(L)OAc (H_2O)]·CoO + 3C CoO + 1C
9	$[Ni(HL)_2Cl_2]\cdot 4H_2O$	42–133 133–550	7.50(7.10) 77.73(78.85)	Loss of water of hydration ($4H_2O$) decomposition of complex and formation of cobalt oxide and carbon	[Ni $(HL)_2Cl_2$]· NiO + 7C
10	$[Ni_2(L)_2(OAc)_2]\cdot 4H_2O$	27–75 75–255 255–899	6.00(6.43) 4.50(4.30) 78.30(77.80)	Loss of water of hydration ($4H_2O$) Loss of one acetato ligand Decomposition of complex	$[Ni_2(L)_2(OAc)_2]$ $[Ni_2(L)_2(OAc)]$ NiO
11	$[Zn(L)_2]\cdot 2H_2O$	45–131 131–999	3.98(3.95)	Loss of water of hydration ($2H_2O$) Decomposition of complex	$[Zn(L_2)]\cdot ZnS$ + 7C
12	$[Fe(HL)_2Cl_2]Cl\cdot H_2O$	55–160 160–350 605–700	1.60 (1.80) 70.30(68.80) 8.97(8.45)	Loss of water of hydration ($1H_2O$) Decomposition of complex and formation of iron sulfide and carbon Oxidation of carbon to CO_2	$[FeCl_2(HL)_2]Cl$ Fe_2S_3 + 7C Fe_2S_3

2.8. Biological Activities

2.8.1. Effect of Ligand 1 and Its Metal Complexes **2**, **7** and **9** on Solid Tumor Volume

Mice bearing solid tumors were treated SC with 0.2 mM of ligand **1** and its metal complexes **2**, **7** and **9**. The treatment was started seven days after EAC implementation in mice and was continued for 14 consecutive days. Tumor volume was measured after 24 h from the last dose of treatment. As shown in Table 6, treatment of solid tumor-bearing mice with the ligand **1** resulted in a significant reduction in tumor volume with inhibition of (36.6%) as compared with tumor-bearing mice treated with DMSO. Metal complexes **2**, **7** and **9** exhibited potent effects on reduction of the volume of solid tumor. The recorded inhibition percents were 66.5%, 70.37% and 75.53%, respectively, as compared with tumor-bearing mice treated with the vehicle.

Table 6. Effect of ligand **1** and its metal complexes **2**, **7** and **9** on the volume of solid tumor.

Groups	Tumor Volume (mm^3)	Inhibition %
Tumor-bearing mice + DMSO	334.8 ± 17.5	-
Tumor-bearing mice + ligand **1**	212.2 ± 22 *	36.6
Tumor-bearing mice + complex **2**	112.2 ± 52 **	66.5
Tumor-bearing mice + complex **7**	99.2 ± 17.9 **	70.37
Tumor-bearing mice + complex **9**	82.6 ± 3.9 **	75.53

Data are presented as mean ± SEM. Significantly (* $p < 0.01$ and ** $p < 0.001$) different from mice bearing solid tumor treated with vehicle (DMSO). -: indicates no value available.

2.8.2. Effect of Ligand **1** and Its Metal Complexes **2**, **7** and **9** on the Biochemical Analysis of Serum

As shown in Table 7, EAC cells induced a significant reduction in albumin and glucose and a significant elevation in alanine aminotransferase (ALT) and aspartate aminotransferase (AST) levels ($p < 0.001$) in comparison with normal mice (normal control group). Conversly, ligand **1** and its metal

complexes **2**, **7** and **9** exhibited significant increase of albumin and glucose levels and decrease ALT and AST levels relative to tumor-bearing mice treated with DMSO (Table 7).

An increase in glucose catabolism and a decrease in glucose synthesis in the presence of cancer cells were reported [70,71]. Therefore, the decrease in serum glucose in mice bearing solid tumor may be due to the tumors exhibit high rate of glycolysis. This is a way of stimulating the body into a constant state of gluconeogenesis which is accompanied with the reduction in serum albumin [72,73]. Treatment of tumor-bearing mice with ligand **1** and its metal complexes, especially complex **7**, restored serum glucose, albumim, ALT and AST levels towards the standard levels when compared with the tumor-bearing mice treated with the vehicle.

Table 7. Effect of ligand **1** and its metal complexes **2**, **7** and **9** on serum biochemical parameters of mice bearing solid tumor.

Groups	ALT (U/L)	AST (U/L)	Albumin (g/dL)	Glucose (mg/dL)
Normal control	39 ± 3.1	194 ± 35.1	3.3 ± 0.3	128 ± 8.8
Solid tumor + DMSO	77.8 ± 11.5 $^{\#}$	438.6 ± 66.4 $^{\#}$	2.5 ± 0.2 $^{\#}$	80.2 ± 9.5 $^{\#}$
Solid tumor + ligand **1**	43.2 ± 9 *	387 ± 45.6 *	2.3 ± 0.3	86.4 ± 11.2
Solid tumor + complex **2**	42.2 ± 5 *	275.6 ± 60.9 *	2.4 ± 0.2	122.2 ± 11.6 **
Solid tumor + complex **7**	39.2 ± 7.9 *	206.6 ± 54.3 **	2.5 ± 0.1	126 ± 9.6 ***
Solid tumor + complex **9**	36.6 ± 3.9 **	208 ± 51.2 **	2.7 ± 0.4	127.4 ± 13.5 **

Data are presented as mean ± SEM. ALT: alanine aminotransferase; AST: aspartate aminotransferase. Significantly ($^{\#}$ $p < 0.01$) different from the normal mice (untreated) and significantly (* $p < 0.05$, ** $p < 0.01$, *** $p < 0.001$) different from mice bearing solid tumor treated with vehicle (DMSO).

2.8.3. Effect of Ligand **1** and Its Metal Complexes **2**, **7** and **9** on the Expression of Vascular Endothelial Growth Factor (VEGF) in Tumor and Liver Tissues of EAC Mice

VEGF is a significant angiogenic factor released during the tumor formation to stimulate the angiogenesis process. Usage of VEGF antagonists is one of the essential anti-angiogenic therapies for cancer treatment [74]. Therefore, the effect of ligand **1** and its metal complexes **2**, **7** and **9** on VEGF expression was studied in tumor and liver tissues of EAC mice. Results as presented in Figure 2A,B illustrated that VEGF is highly expressed in tumor and liver tissues of mice bearing solid tumor compared to normal mice.

The increasing in the VEGF expression level in mice bearing solid tumors was related to the presence of EAC cells. This finding is consistent with previously reported results which concluded that EAC cells has been found to exhibit strong VEGF expression level [75]. Moreover, cancer usually enhances VEGF expression through tumor aggression, therefore, VEGF is involved in cancer pathology [76]. Conversely, the treatment with ligand **1** and its metal complexes **2**, **7** and **9** downregulated the expression of VEGF in tumor (Figure 2A) and in liver tissues (Figure 2B) of mice bearing solid tumor in comparison to mice bearing solid tumor treated with DMSO. Complex **9** exhibited the most potent anti-VEGF activity among the tested compounds. These results revealed that the anti-tumor activities of the tested compounds might be due to their ability to inhibit VEGF.

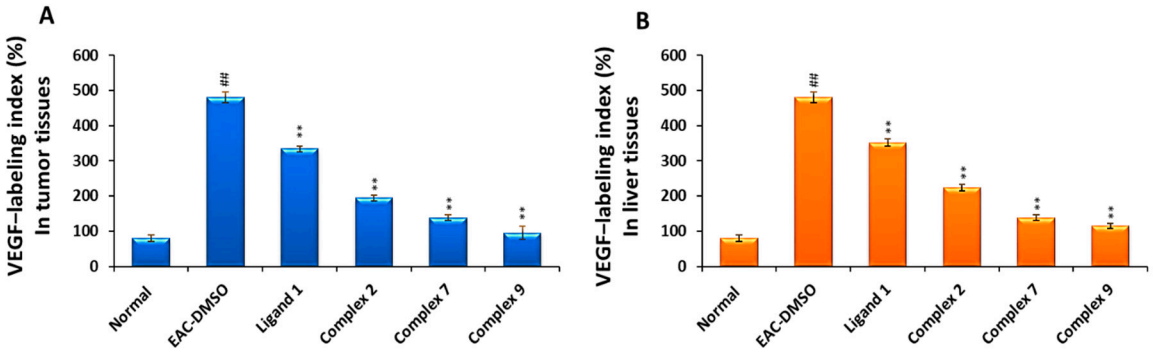

Figure 2. Effect of ligand **1** and its metal complexes **2**, **7** and **9** on vascular endothelial growth factor (VEGF) expression in tumor tissues (**A**) and in liver tissues (**B**) of Ehrlich ascites carcinoma (EAC)-bearing mice. VEGF expression was determined by immunohostochemistry assay. VEGF expression was expressed as labeling index percentage. Data are expressed as mean ± SEM. Significantly (## $p < 0.01$) different from the normal mice and significantly (** $p < 0.01$) different from mice bearing solid tumor treated with vehicle (DMSO).

2.8.4. Effect of Ligand **1** and Its Metal Complexes **2**, **7** and **9** on the Expression of Cysteine Aspartyl-Specific Protease-7 (Caspase-7) in Tumor and Liver Tissues of EAC Mice

Apoptosis is a programmed cell death that is caused by caspases that target cysteine aspartyl residues in target proteins [77]. Defects in apoptosis mechanisms can induce tumor pathogenesis [78], for example, the activation of caspases by the signal transduction pathway can lead to irreversible apoptosis through protein degradation [79]. Therefore, it is important to design and develop new agents that act as caspases activators to treat cancers [80,81]. Consequently, the effect of ligand **1** and its metal complexe **2**, **7** and **9** on the stimulation of caspase-7 was examined in tumor and liver tissues of EAC mice.

As shown in Figure 3A,B, the induction of solid tumors is associated with low expression of caspase-7 in tumor and liver tissues of mice bearing solid tumor compared to normal mice. Our finding was compatible with the reported data demonstrating the declined expression of caspase-3 in mice bearing EAC cells [82]. On the other hand, the treatment with ligand **1** and its metal complexes **2**, **7** and **9** upregulated the expression of caspase-7 in tumor (Figure 3A) and in liver tissues (Figure 3B) of mice bearing EAC tumor in comparison to mice bearing solid tumor treated with DMSO.

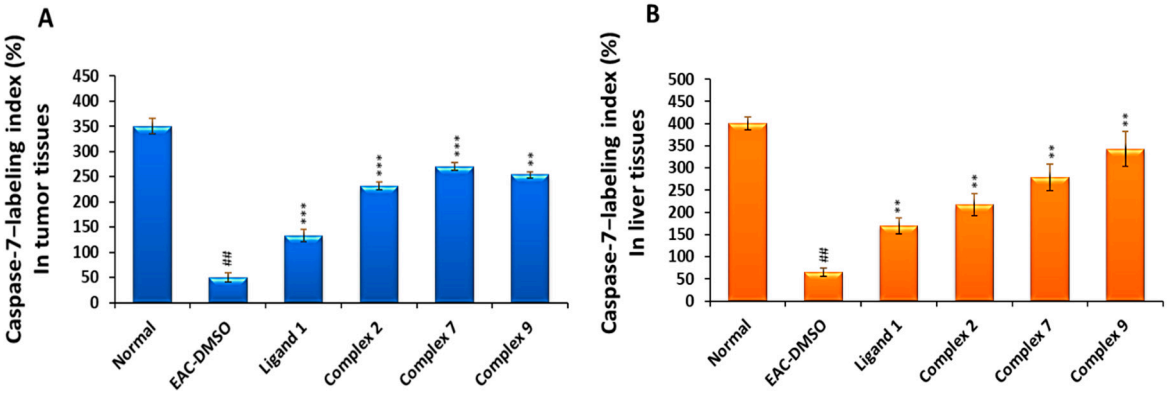

Figure 3. Effect of ligand **1** and its metal complexes **2**, **7** and **9** on cysteine aspartyl-specific protease-7 (caspase-7) expression in tumor tissues (**A**) and in liver tissues (**B**) of Ehrlich ascites carcinoma (EAC)-bearing mice. Caspase-7 expression was determined by immunohistochemistry assay. Caspase-7 expression was expressed as labeling index percentage. Data are expressed as mean ± SEM. Significantly ($^{##}$ $p < 0.01$) different from the normal mice and significantly (** $p < 0.01$ and *** $p < 0.001$) different from mice bearing solid tumor treated with vehicle (DMSO).

Complex **9** followed by complex **7** exhibited the most potent apoptotic activity among the tested compounds. Caspase-7 is a critical mediator of apoptosis and the overexpression of it induced apoptosis of cancer cells [83]. Therefore, these results revealed that the anti-tumor activities of the tested compounds might be due to their ability to stimulate caspase-7.

3. Materials and Methods

3.1. Chemistry

3.1.1. Preparation of *N*(4)-antipyrinylthiosemicarbazide

The preparation of S-methylantipyrine carbodithioate was illustrated in Scheme 1. In details, 4-Aminoantipyrine (40.6 g, 0.2 mol) was added in small portions to an aqueous KOH solution (11.2 g, 100 mL), and the mixture was maintained below 5 °C using ice. Refrigerator-cooled CS_2 (11.36 cm^3, 0.2 mol) was then added dropwise to the stirred solution over l h while the solution was maintained below 10 °C. To the resulting yellow solution, MeI (11.68 cm^3, 0.2 mol) dropwise was added over 2 h while the temperature was maintained below 10 °C. During the addition of MeI, the yellow colour of the mixture gradually diminished, and a white solid powder was formed. The crystals of S-methyl-antipyrinecarbodithioate were collected by vacuum filtration and washed with cold H_2O. Because of the noxious odour of this solid (m.p. 193 ± 2 °C), it was used immediately without purification.

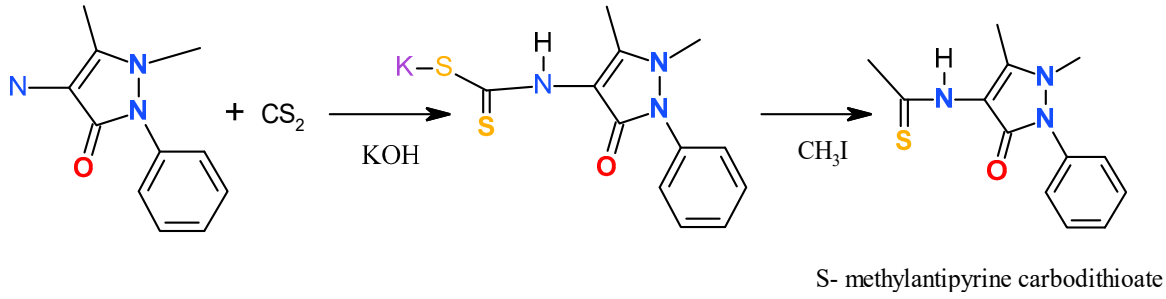

Scheme 1. Preparation of *S*-methylantipyrine carbodithioate.

The preparation of N(4)-antipyrinylthiosemicarbazide was presented in Scheme 2. *S*-Methylantipyrinecarbodithioate (29.3 g, 0.1 mol) dissolved in EtOH (30 mL) was added to hydrazine monohydrate (3.2 mL, 0.1 mol). The solution was heated at reflux until the evolution of methyl mercaptan was almost complete. The release of methyl mercaptan was detected based on the yellow colour it imparts to paper moistened with $Pb(OAc)_2$ placed at the mouth of the condenser. The reaction time for this step was 8 h. The resulting white solid crystals, *N*(4)-antipyrinyl-thiosemicarbazide, were collected by vacuum filtration, washed with cold i-PrOH and dried (m.p. 203 ± 2 °C).

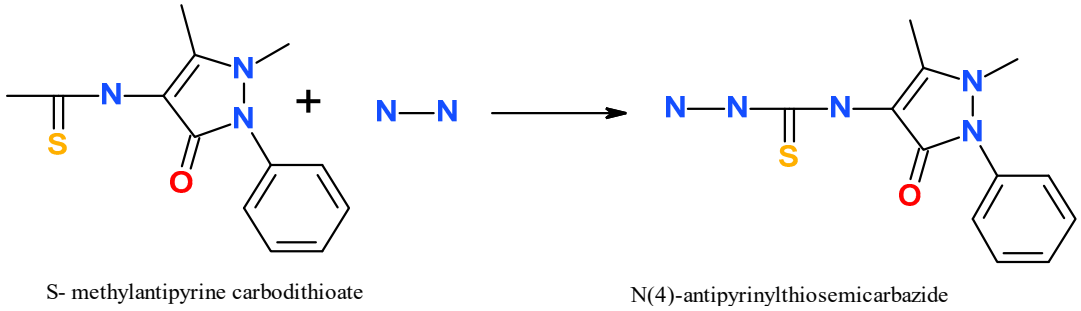

Scheme 2. Preparation of *N*(4)-antipyrinylthiosemicarbazide.

3.1.2. Preparation of Isatin *N*(4)-antipyrine-thiosemicarbazide **1** (ligand)

Isatin N(4)-antipyrine-thiosemicarbazide **1** (ligand) was prepared by mixing equimolar amounts of isatin and *N*(4)-antipyrine-thiosemicarbazide in anhydrous EtOH with a few drops of concentrated H_2SO_4 at reflux (80 °C) for 2 h as shown in Scheme 3.

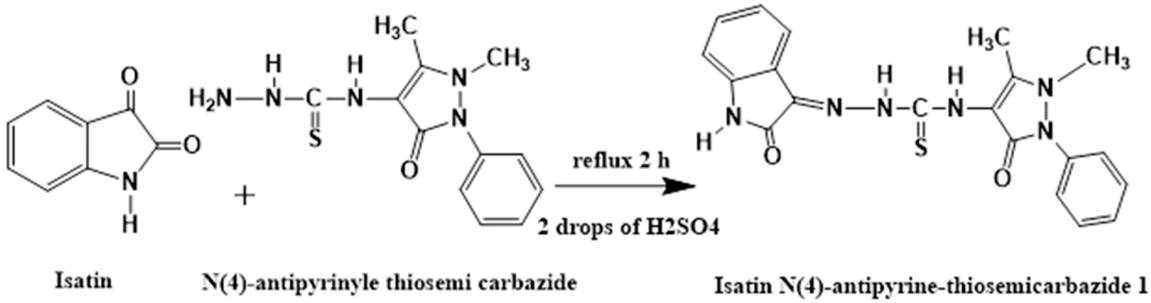

Scheme 3. Preparation of Isatin *N*(4)-antipyrine-thiosemicarbazide **1** (ligand).

Ligand **1**: Yield (87%), m.p. = 210–212 °C; color: yellow, Elemental analysis for $C_{20}H_{18}N_6O_2S$, (F.W. = 406.): Found (calcd) %C 59.14 (59.00), %H 5.15(4.43), %N 20.91(20.66), %S 7.85(7.87)); IR (KBr, cm^{-1}), 3442, 3348, 3287, 3251, 3141ν(NH), 1738 ν(C=O)$_{isatin}$, 1645 ν(C=O)$_{antipyrine}$, 1688, 1623, 1595 ν(C=N), 881 ν(C=S); UV-Vis. (Nujol mulls) (nm) 268, 280, 369 nm, ^{1}H-NMR (MHz, DMSO-d_6, δ, ppm): 12. 819 (s, 1 H, thiosemicabazide N-NH), 11.219 (s, 1H, indole N-H), 10.115 (s, 1H, CS-N-H), 7.702–6.876. (m, multiple, H aromatic protons), 3.068 (s, 3 H, N-CH_3), 2.135 (s, 3 H, CH_3). GC–MS: *m*/*z* (relative abundance); 406.27, 363.47 (27.15), 291 (100), 276.68 (72.92), 261.69 (28.97), 223.71 (90.05), 204.07 (22.73), 203.3 (26.0), 145.64 (51.57), 130.57 (28.60), 118.18 (78.92), 67.30 (18.68).

3.1.3. Preparation of the Metal Complexes

The metal complexes of the ligand were prepared by mixing a hot ethanolic solution (30 mL) of the metal salt ($CuCl_2{\cdot}2H_2O$, $CuBr_2$, $Cu(NO_3)_2{\cdot}3H_2O$, $Cu(OAc)_2{\cdot}H_2O$, $Cu(ClO_4)_2$, $CoCl_2{\cdot}6H_2O$, $Co(OAc)_2{\cdot}4H_2O$, $NiCl_2{\cdot}6H_2O$, $Ni(OAc)_2{\cdot}4H_2O$, $ZnCl_2$ and $FeCl_3{\cdot}6H_2O$) with the appropriate amount of a hot (75 °C) ethanolic solution of the ligand to form a 1:1 L/M (ligand/metal) solution. The reaction mixture was then refluxed for approximately 2 h. The obtained precipitates were separated by filtration, washed several times with ethanol and then diethyl ether, and then dried under vacuum over anhydrous $CaCl_2$. Due to the poor solubility of these complexes in most organic solvents and water, all attempts to prepare a single crystal of the ligand or any of the metal complexes were unfortunately unsuccessful.

[Cu(L)Cl]·H_2O (**2**): Yield (79%), m.p. = 238–240 °C; color: dark brown, Λ_M: 10.0 ohm^{-1} cm^2 mol^{-1}, Elemental analysis for $C_{20}H_{19}N_6O_3SCuCl$., (F.W. = 522.6): Found (calcd) %C 46.0(46.0), %H 4.1(3.64), %N 16.3(16.10), %S 6.88(6.13): IR (KBr, cm^{-1}), 3395 ν(H_2O), 3161, 3100 ν(NH), 1702 ν(C=O)$_{isatin}$, 1645 ν(C=O)$_{antipyrine}$, 1616, 1539 ν(C=N), 808 ν(C=S), 632 ν(Cu-O), 498 ν(Cu-N) UV-Vis. (Nujol mulls) (nm) 310, 325 n→π*, 395, 460, 525 Charge transfer, 600, 672, 725 d→d, μ_{eff} (B.M) = 1.83.

[Cu(L)Br]·3H_2O (**3**): Yield (89%), m.p. = 250 °C; color: brown, Λ_M: 37.9 ohm^{-1} cm^2 mol^{-1}, Elemental analysis for, $C_{20}H_{23}N_6O_5SCuBr$, (F.W. = 602.5): Found (calcd) %C 38.81(39.83), %H 3.54(3.82), %N 15.02(13.94), %S 5.03(5.31) IR (KBr, cm^{-1}), 3446 ν(H_2O), 3106ν(NH), 1695 ν(C=O)$_{isatin}$, 1643 ν(C=O)$_{antipyrine}$, 1622, 1578 ν(C=N), 806 ν(C=S), 614 ν(Cu-O), 504 ν(Cu-N); UV-Vis. (Nujol mulls) (nm) 325 n→π*, 380, 445, 500 charge transfer, 580, 631, 660 d→d, μ_{eff} (B.M) = 1.81.

[Cu(L)(NO_3)]·H_2O (**4**): Yield (80%), m.p. = 247 °C; color: brown, Λ_M: 34.3 ohm^{-1} cm^2 mol^{-1}, Elemental analysis for, $C_{20}H_{19}N_7O_6SCu$, (F.W. = 548.5): Found (calcd) %C 43.4(43.5), %H 3.29(3.50), %N 18.0(17.9), %S 6.0(5.8); IR (KBr, cm^{-1}), 3425ν(H_2O), 3166ν(NH), 1703 ν(C=O)$_{isatin}$, 1645 ν(C=O)$_{antipyrine}$, 1620, 1539 ν(C=N), 1382,1462 ν(NO3), 808 ν(C=S), 638 ν(Cu-O), 586 ν(Cu-N); UV-Vis. (Nujol mulls) (nm) 310 n→π*, 390, 455, 520, 574 charge transfer, 675, 720 d→d, μ_{eff} (B.M) = 1.78.

[Cu(L)OAc]·2H$_2$O (**5**): Yield (74%), m.p. = 212–216 °C; color: brown, Λ_M: 11.9 ohm^{-1} cm^2 mol^{-1}, Elemental analysis for, $C_{22}H_{24}N_6O_6SCu$, (F.W. = 563.5): Found (calcd) %C 46.12(46.90), %H 4.82(4.30), %N 15.13 (14.9), %S 5.1(5.7); IR (KBr, cm^{-1}), 3417 ν(H$_2$O), 3237ν(NH), 1680 ν(C=O)$_{isatin}$, 1645 ν(C=O)$_{antipyrine}$, 1560, 1525 ν(C=N), 1615, 1333 ν(OAc), 847 ν(C=S), 595 ν(Cu-O), 503 ν(Cu-N); UV-Vis. (Nujol mulls) (nm) 310 n→π*, 395, 430, 460, 560 charge transfer, 671,740(br), 870 d→d, μ_{eff} (B.M) = 1.79.

[Cu(L)ClO$_4$]·2H$_2$O (**6**): Yield (91%), m.p. = 250–252 °C; color: brown, Λ_M: 45.50 ohm^{-1} cm^2 mol^{-1}; Elemental analysis for, $C_{20}H_{21}N_6O_8SCuCl$, (F.W. = 604.5): Found (calcd) %C 38.92(39.70), %H 3.75(3.48), %N 14.67(13.91), %S 5.18(5.29); IR (KBr, cm^{-1}), 3428 ν(H$_2$O), 3325, 3170ν(NH), 1628 ν(C=O)$_{isatin}$, 1645 ν(C=O)$_{antipyrine}$, 1568, 1516ν(C=N), 1118,1085, 694,631 ν(ClO4), 838 ν(C=S), 693 ν(Cu-O), 505 ν(Cu-N); UV-Vis. (Nujol mulls) (nm) 310 n→π*, 357, 390, 480(br) charge transfer, 790(br) d→d, μ_{eff} (B.M) = 1.76.

[Co(L)Cl]$_2$·2H$_2$O (**7**): Yield (66%), m.p. = 258–260 °C; color: brown, Λ_M: 17.9 ohm^{-1} cm^2 mol^{-1}, Elemental analysis for $C_{40}H_{38}N_{12}O_6S_2Co_2Cl_2$, (F.W. = 1034.8): Found (calcd) %C 47.0(46.38), %H 4.17(3.7), %N 17.0(16.21), %S .4(6.18), IR (KBr, cm^{-1}), 3388 ν(H$_2$O), 3150 ν(NH), 1734 ν(C=O)$_{isatin}$, 1645 ν(C=O)$_{antipyrine}$, 1600, 1515 ν(C=N), 841 ν(C=S), 585 ν(Co-N); GC–MS: *m*/*z* (relative abundance); 999.5 (22.46), 869.45 (15.13), 464.94 (4.00); UV-vis. (Nujol mulls) (nm) 318, 345 n→π*, 390, 450(br) charge transfer, 600, 675, 700 d→d, μeff (B.M) = 3.1.

[Co(L)OAc(H$_2$O)]·4H$_2$O (**8**): Yield (75%), m.p. > 300 °C; color: brown, Λ_M: 4.6 ohm^{-1} cm^2 mol^{-1}, Elemental analysis for $C_{22}H_{30}N_6O_9SCo$, (F.W. = 612.5): Found (calcd) %C 42.96(43.10), %H 5.3(4.89),%N 14.20(13.71), %S 4.87(5.22); IR (KBr, cm^{-1}), 3491, 3422 ν(H$_2$O), 3196ν(NH), 1734 ν(C=O)$_{isatin}$, 1645 ν(C=O)$_{antipyrine}$, 1590, 1545 ν(C=N), 1619, 1372 ν(OAc), 841 ν(C=S), 540 ν(Co-N); GC–MS: *m*/*z* (relative abundance); 612.85 (100), 576.23 (94.07, 561.30 (61.93), 541.85 (6.86), 523.22 (39.20); UV-Vis. (Nujol mulls) (nm) 320 n→π*, 390, 440(br), 530(br) charge transfer, 600, 675, 780d→d, μ_{eff} (B.M) = 3.7

[Ni(HL)$_2$Cl$_2$]·4H$_2$O (**9**): Yield (84%), m.p. = 254–255 °C; color: brown, Λ_M: 13.5 ohm^{-1} cm^2 mol^{-1}, Elemental analysis for $C_{40}H_{44}N_{12}O_8S_2$ $NiCl_2$., (F.W. = 1014.9): Found (calcd) %C 46.84(47.3), %H 4.94(4.33), %N 16.95(16.55), %S 5.89(6.30); IR (KBr, cm^{-1}), 3441 ν(H$_2$O), 3280 ν(NH), 1735, 1660 ν(C=O)$_{isatin}$, 1645, 1620 ν(C=O)$_{antipyrine}$, 1595(sh), 1520(sh) ν(C=N), 880 ν(C=S), 648 ν(Ni-O), 591 ν(Ni-N); UV-VIS. (Nujol mulls) (nm) 320 n→π*, 396, 420, 530 charge transfer, 560(s), 690(w), 950(br) d→d, μ_{eff} (B.M) = 2.98.

[Ni(L)OAc]$_2$·4H$_2$O (**10**): Yield (70%), m.p. > 300 °C; color: brown, Λ_M: 2.60 ohm^{-1} cm^2 mol^{-1}, Elemental analysis for $C_{44}H_{48}N_{12}O_{12}S_2$ Ni_2, (F.W. = 1017.4): Found (calcd) %C 47.76(47.24), %H 4.19(4.3), %N, 15. 60(15.03), %S 6.71(5.78); IR (KBr, cm^{-1}), 3445 ν(H$_2$O), 3310, 3200 ν(NH), 1664 ν(C=O)$_{isatin}$, 1620 ν(C=O)$_{antipyrine}$, 1580, 1540 ν(C=N), 1620, 1342 ν(OAc), 829 ν(C=S), 590 ν(Ni-O), 503 ν(Ni-N); UV-Vis. (Nujol mulls) (nm) 305, 315 n→π, 395, 450, 530 charge transfer, 567(s), 670(sh). 950(br) d→d, μ_{eff} (B.M) = 3.06.

[Zn(L)$_2$]·2H$_2$O (**11**): Yield (69%), m.p. > 300 °C; color: dark yellow, Λ_M: 1.40 ohm^{-1} cm^2 mol^{-1}, Elemental analysis for $C_{40}H_{38}N_{12}O_6S_2$ Zn, (F.W. = 911.50): Found (calcd) %C 51.9(52.6), %H 3.7 (4.2), %N 18.8 (18.42), %S 6.64 (7.0); IR (KBr, cm^{-1} 3413 ν(H$_2$O), 3223ν(NH), 1700 ν(C=O)$_{isatin}$, 1643 ν(C=O)$_{antipyrine}$, 1609, 1570 ν(C=N), 815 ν(C=S), 612 ν(Zn-O), 580 ν(Zn-N): ^{1}H-NMR (MHz, DMSO-d_6, δ, ppm): 11.22 (s, 1H, indole N-H), 11.008 (s,1H, CS-N-H), 7.704–6.879. (m, multiple, C-H aromatic), 3.111 (s, 3 H, N-CH3), 2.174 (s, 3 H, CH3); GC–MS: *m*/*z* (relative abundance); 911.5 (1.19) UV-Vis. (Nujol mulls) (nm) 319 n→π, 396, 440, 491, 520(sh).

[Fe(HL)$_2$Cl$_2$]Cl·H$_2$O (**12**): Yield (78%), m.p. = 210–212 °C; color: dark green, Λ_M: 74.50 ohm^{-1} cm^2 mol^{-1}, Elemental analysis for $C_{40}H_{38}N_{12}O_5S_2FeCl_3$, (F.W. = 992.50): Found (calcd) %C 47.62(48.3), %H 3.9(3.8), %N 16.95 (16.91), %S 5.6 (6.44), IR (KBr, cm^{-1}), 3429(s,br) ν(H$_2$O), 3280 ν(NH), 1737, 1700 ν(C=O)$_{isatin}$, 1645, 1621 ν(C=O)$_{antipyrine}$, 1610, 1576 ν(C=N), 880 ν(C=S), 589 ν (Fe-O), 512 ν(Fe-N) GC–MS: *m*/*z* (relative abundance); 992.5 (11.39), 974.50 (1.90), 938.30 (12.96), 869.80 (8.27), 464.40 (2.48); UV-Vis. (Nujol mulls) (nm) 300, 340 n→π, 391, 450, 530(sh) charge transfer, 567(s), 584 d→d, μ_{eff} (B.M) = 5.95.

3.1.4. Instrumentation and Measurements

Elemental microanalyses [C, H, and N] were conducted in the Micro Analytical Unit. The IR spectra were acquired using KBr discs in a Spirit model FT-IR spectrophotometer (Shimadzu, Thermo Scientific, Glasgow, UK). The ^{1}H-NMR spectra of the ligand and zinc complex were recorded in DMSO-d_6 on a Gemini 200 NMR spectrophotometer (Varian, Palo Alto, CA, USA) at 300 MHz. Mass spectra were collected using a model ISQLT direct probe controller with a single quadrupole mass analyser (Thermo Scientific, Glasgow, UK) using Thermo X-calibur software (Xcalibur 4.1). Solid-state electronic spectra were recorded in Nujol mulls using a Shimadzu UV-Vis 1800 spectrophotometer (Thermo Scientific, Glasgow, UK). The molar conductance of a 1×10^{-3} M solution of the complexes in *N*,*N*-dimethylformamide (DMF) was measured at 25 °C with a Bibby MCl-type conductometer (Chelmsford, UK). The resistance was measured in ohms and the molar conductivities were calculated according to the following equation: ΛM = VxKxg/Mw* Ω where ΛM = molar conductivity (Ω-1cm2mol-1), V = volume of the complex solution (mL), K = cell constant (0.92 cm-1), Mw = molecular weight of the complex, g = weight of the complex (g), and Ω = resistance (Ω).

The solid-state electron paramagnetic resonance (EPR) spectra of the copper(II) complexes were recorded with an X-band EMX spectrometer (Bruker, Berlin, Germany) using a standard rectangular cavity of ER 4102 operating at 9.5 GHz with 100 kHz modulation at 298 K. Diphenyl picryl hydrazide (DPPH) was used as a g-marker to calibrate the spectra. The thermal analyses (TGA) were carried out in air using a Shimadzu DT-30 thermal analyser. Magnetic susceptibilities were measured at 27 °C using the modified Gouy method with a Johnson Matthey balance and were calculated using the following equation:

$$Meff = 2.84\sqrt{x_m^{corr} \cdot T}$$

3.2. Biological Evalution

3.2.1. Preparation of Solutions of the Complexes

Stock solutions (1 mM) of the newly synthesized complexes were prepared by dissolving each complex in dimethylsulfoxide (DMSO)/H_2O, and the solutions were stored at 4 °C. Only ligand 1 and complexes **2**, **7** and **9** were successfully solubilized, allowing their antitumor activities to be determined.

3.2.2. Experimental Animals

Adult female Swiss albino mice (6–7 weeks old), weighing 20–22 g, were purchased and housed under standard ventilation and light cycle conditions. They were given food and water ad libitum. The current study protocol was approved by the Ethical Committee for Laboratory Animals of Science Faculty Menoufia University (No.: ECLA-SFMU-18015).

3.2.3. Tumor Cell Line

The Ehrlich ascites carcinoma (EAC) cell line was purchased from the National Cancer Institute (NCI, Cairo, Egypt). The EAC cell line was maintained in the peritoneal cavity of adult female Swiss albino mice by serial intraperitoneal transplantation of 2.5×10^6 cells weekly.

3.2.4. Induction of Solid Tumor and Animals Grouping

The solid tumor was induced by subcutaneously (SC) injecting 1×10^{-6} EAC cells into the right thigh of the lower limb of mice [84,85]. Seven days after tumor inoculation, the tumor volume became palpable. The mice were randomly divided in separate cages into six groups:

Group 1 (normal control): mice without any treatment.
Group 2 (vehicle group): mice bearing solid tumors treated with DMSO/H_2O.
Group 3: mice bearing solid tumor and treated subcutaneously with 0.2 mM of ligand **1**.
Group 4: mice bearing solid tumor and treated subcutaneously with 0.2 mM of complexe **2**.

Group 5: mice bearing solid tumor and treated subcutaneously with 0.2 mM of complexe **7**.
Group 6: mice bearing solid tumor and treated subcutaneously with 0.2 mM of complexe **9**.

The doses were selected based on the LD_{50} values of the complexes (data not shown). The treatment was started seven days after EAC implementation and was continued for 14 consecutive days.

3.2.5. Blood and Tissue Samples Collection

At the end of the experiment, mice were sacrificed. Blood samples were collected from jugular vein puncture into chilled non-heparinized tubes, which were centrifuged at 40× *g* for 10 min at 4 °C. The sera were frozen at −20 °C for future measurements. The livers and solid tumors were removed and cut into pieces, and the individual pieces were fixed in paraffin blocks for immunohistochemical assays.

3.2.6. Assessment of Tumor Volume (TV)

After 24 h from the last dose of treatment, mice were sacrificed and the solid tumors were carefully removed. The volume of the tumors was assessed [86] using the following formula: TV (mm^3) = 4π $(A/2)^2 \times (B/2)$, where (A) is the minor tumor axis and (B) is the major tumor axis.

3.2.7. Biochemical Analysis of the Serum

To determine the effect of ligand **1** and its metal complexes **2**, **7** and **9** on the serum biochemical profile. The levels of alanine transaminase (ALT), aspartate transaminase (AST), albumin and glucose were determined using a Beckman autoanalyzer apparatus, Brea, CA, USA).

3.2.8. Immunohistochemical Examination of VEGF and Caspase-7 in Solid Tumors and Liver Tissues

The effect of ligand **1** and its metal complexes **2**, **7** and **9** on the expression of VEGF and caspase-7 in solid tumor tissues and in liver tissues of mice bearing solid tumors was deremined by immunohistochemical methods. In details, the sections of tumor and liver tissues in paraffin were dewaxed, hydrated, and immersed in antigen retrieval solution (EDTA solution, pH 8). The samples were treated with 0.3% hydrogen peroxide and protein block and then incubated with anti-VEGF (Santa Cruz, Dallas, TX, USA, 1:100 dilution) and anti-caspase-7 (Lab Vision, Thermo Fischer Scientific, Glasgow, UK; ready to use) at 4 °C overnight. The slides were rinsed three times with PBS and incubated with anti-mouse IgG secondary antibodies (EnVision + System HRP; Dako, SanJose, CA, USA) for 30 min at room temperature. The samples were visualized with diaminobenzidine commercial kits (Liquid DAB+Substrate Chromogen System; Dako) and finally counterstained with Mayer's haematoxylin. In the negative control, the primary antibody was replaced with normal mouse serum. The positive cells were counted from seven high-power fields of 400×. The labelling index (%) was determined by dividing the number of positive cells by the total cells × 100 [87,88].

3.3. Statistical Analysis

Data are expressed as mean ± SEM and the statistical comparison between groups were analyzed using one-way ANOVA followed by Tukey post hoc test. A p of < 0.05 value was considered statistically significant.

4. Conclusions

In summary, new metal complexes derived from isatin-N-(4)antipyrinethiosemicarbazone ligand **1** were synthesized and characterized. Also, their potential anti-cancer activities against solid tumors induced by EAC cells in mice were investigated. The results revealed that the tested complexes significantly reduced the volume of solid tumors. This reduction was associated with an increase in the level of caspase-7 and a dramatic decrease in the VEGF level. The tested complexes are promising anti-cancer agents those exert their activities via the induction of apoptosis and the inhibition of angiogenesis, leading to reduction of the tumor size.

Supplementary Materials: The following are available online; ^{1}H-NMR, Mass, IR, EPR, TGA, and UV-Visible spectra.

Author Contributions: Conceptualization, F.E.-S., B.E.-A. and T.S.; Formal analysis, B.E.-A. and F.E.-S.; Funding acquisition, S.A.M.K. and H.R.E.-S.; Methodology, B.E.-A., and G.S.; Visualization, B.E.-A. and F.E.-S.; Writing—original draft, B.E.-A., F.E.-S., and G.S.; Writing—review & editing, B.E.-A., G.S., S.A.M.K., and H.R.E.-S. All authors have read and approved the manuscript.

Funding: We are very grateful to the Swedish Research links grant 2016-05885 (VR for the years 2017–2019) for generious financial support.

Acknowledgments: H.R.E.-S. is very grateful to Jiangsu University, China for Foreign Expert fellowship.

Conflicts of Interest: The authors declare no conflict of interest.

References

1. Siegel, R.L.; Miller, K.D.; Jemal, A. Cancer statistics, 2019. *CA* **2019**, *69*, 7–34. [CrossRef] [PubMed]
2. Folkman, J. Angiogenesis in cancer, vascular, rheumatoid and other disease. *Nat. Med.* **1995**, *1*, 27–30. [CrossRef] [PubMed]
3. Thapa, D.; Lee, J.S.; Heo, S.W.; Lee, Y.R.; Kang, K.W.; Kwak, M.K. Novel hexahydrocannabinol analogs as potential anti-cancer agents inhibit cell proliferation and tumor angiogenesis. *Eur. J. Pharmacol.* **2011**, *650*, 61–71. [CrossRef] [PubMed]
4. El-Aarag, B.Y.; Kasai, T.; Zahran, M.A.; Zakhary, N.I.; Shigehiro, T.; Sekhar, S.C.; Agwa, H.S.; Mizutani, A.; Murakami, H.; Kakuta, H.; et al. In vitro anti-proliferative and anti-angiogenic activities of thalidomide dithiocarbamate analogs. *Int. Immunopharmacol.* **2014**, *21*, 283–292. [CrossRef] [PubMed]
5. El-Aarag, B.; Kasai, T.; Masuda, J.; Zahran, M.; Agwa, H.; Seno, M. Anticancer effects of novel thalidomide analogs in A549 cells through inhibition of vascular endothelial growth factor and matrix metalloproteinase-2. *Biomed. Pharmacother.* **2017**, *85*, 549–555. [CrossRef] [PubMed]
6. Zahran, M.; Agwa, H.; Osman, A.; Hammad, S.; El-Aarag, B.; Ismail, N.; Salem, T.; Gamal-Eldeen, A. Synthesis and biological evaluation of phthalimide dithiocarbamate and dithioate derivatives as anti-proliferative and anti-angiogenic agents-I. *Eur. J. Chem.* **2017**, *8*, 391–399. [CrossRef]
7. Kamal, A.; Kumar, G.B.; Nayak, V.L.; Reddy, V.S.; Shaik, A.B.; Reddy, M.K. Design, synthesis and biological evaluation of imidazopyridine/imidazopyrimidine-benzimidazole conjugates as potential anticancer agents. *Med. Chem. Commun.* **2015**, *6*, 606–612. [CrossRef]
8. Yang, L.L.; Lee, C.Y.; Yen, K.Y. Induction of apoptosis by hydrolyzable tannins from Eugenia jambos L. on human leukemia cells. *Cancer Lett.* **2000**, *157*, 65–75. [CrossRef]
9. Rosu, T.; Negoiu, M.; Pasculescu, S.; Pahontu, E.; Poirier, D.; Gulea, A. Metal-based biologically active agents: Synthesis, characterization, antibacterial and antileukemia activity evaluation of Cu(II), V(IV) and Ni(II) complexes with antipyrine-derived compounds. *Eur. J. Med. Chem.* **2009**, *45*, 774–781. [CrossRef]
10. Leovac, V.M.; Bogdanovic, G.A.; Jovanovic, L.S.; Joksovic, L.C.; Markovic, I.; Joksovic, M.D. Synthesis, characterization and antitumor activity of polymeric copper(II) complexes with thiosemicarbazones of 3-methyl-5-oxo-1-phenyl-3-pyrazolin-4-carboxaldehyde and 5-oxo-3-phenyl-3-pyrazolin-4-carboxaldehyde. *J. Inorg. Biochem.* **2011**, *105*, 1413–1421. [CrossRef] [PubMed]
11. Refata, M.S.; El-Metwaly, N.M. El-Metwaly, Spectral, thermal and biological studies of Mn(II) and Cu(II) complexes with two thiosemicarbazide derivatives. *Spectrochim. Acta Part A* **2012**, *92*, 336–346. [CrossRef] [PubMed]
12. Mendes, I.C.; Moreira, J.P.; Mangrich, A.S.; Balena, S.P.; Rodrigues, B.L.; Beraldo, H. Coordination to copper (II) strongly enhances the in vitro antimicrobial activity of pyridine-derived *N*(4)-tolyl thiosemicarbazones. *Polyhedron* **2007**, *26*, 3263–3270. [CrossRef]
13. Vinuelas-Zahinos, E.; Maldonado-Rogado, M.A.; Luna-Giles, F.; Barros-Garcia, F.J. Coordination behaviour of Schiff base 2-acetyl-2-thiazoline hydrazone (ATH) towards cobalt(II), nickel(II) and copper(II). *Polyhedron* **2008**, *27*, 879–886. [CrossRef]
14. Bharti, N.; Shailendra, Y.; Sharma, S.; Naqvi, F.; Azam, A. New palladium(II) complexes of 5-nitrothiophene-2-carboxaldehyde thiosemicarbazones. synthesis, spectral studies and in vitro anti-amoebic activity. *Bioorg. Med. Chem.* **2003**, *11*, 2923–2929. [CrossRef]

15. El-Sawaf, A.K.; West, D.X.; El-Saied, F.A.; El-Bahnasawy, R.M. Synthesis, magnetic and spectral studies of iron(III), cobalt(II,III), nickel(II), copper(II) and zinc(II) complexes of 4–formylantipyrine N(4)-antipyrinylthiosemicarbazone. *Transit. Met. Chem.* **1998**, *23*, 649–655. [CrossRef]
16. El-Sawaf, A.K.; West, D.X.; El-Saied, F.A.; El-Bahnasawy, R.M. Copper(II) complexes of 4-formylantipyrine *N*(4)-substitutedthiosemicarbazones. *Transit. Met. Chem.* **1998**, *22*, 360–365. [CrossRef]
17. Ali, A.Q.; Teoh, S.G.; Salhin, A.; Eltayeb, N.E.; Ahamed, M.B.K.; Majid, A.A. Synthesis of isatin thiosemicarbazones derivatives: In vitro anti-cancer, DNA binding and cleavage activities. *Spectrochim. Acta A* **2014**, *125*, 440–448. [CrossRef] [PubMed]
18. El-Saied, F.A.; El-Enein, S.A.A.; Emam, S.M.; El-Shater, H.A. Synthesis and characterization of Cu(II), Ni(II), Co(II), Mn(II), Zn(II), Ru(III), Hf(IV) and ZrO(II) complexes of 2-thiophenylidene-N-4-methoxy anilinoacetohydrazone. *Polish J. Chem.* **2009**, *83*, 1871–1883.
19. Detrov, I.; Grupce, O.; Stafilov, T. The N-H stretching region of some imides and thioimides. *Mol. Struct.* **1986**, *142*, 275–278.
20. Castineiras, A.; Gomez, M.C.; Sevillano, P. 2-(2,3-Dihydro-1,3-benzothiazol-2-yl)phenyl(diphenyl) phosphine oxide, Synthesis and characterization by IR and NMR spectroscopy and X-ray diffractometry. *Mol. Struct.* **2000**, *554*, 301–306. [CrossRef]
21. Prasad, R.N.; Mathur, M.; Upadhayay, A. Synthesis and spectroscopic studies of Cr (III), Fe (III) and Co (II) complexes of hexaazamacrocycles. *Indian Chem. Soc.* **2007**, *84*, 1202–1204.
22. Husain, K.; Bhat, A.; Azam, A. New Pd(II) complexes of the synthesized 1-N-substituted thiosemicarbazones of 3-indole carboxaldehyde: Characterization and antiamoebic assessment against E. histolytica. *J. Med. Chem.* **2008**, *43*, 2016–2028. [CrossRef] [PubMed]
23. Mikuriya, M.; Okawa, H.; Kida, S. Binuclear Metal Complexes. XXXV. Synthesis and Magnetism of Binuclear Copper(II) Complexes with 3-[2-(Dialkylamino)ethylthio]-1-propanols. *Bull. Chem. Soc.* **1980**, *53*, 3717–3718. [CrossRef]
24. Rreti, C.; Tosr, G. Complexes of Co alt (II), Nickel (II) and Copper Acetates, Perchlorates, and Tetrafluoroborates with Heterocyclic Ligands Containing VA and VIA group Donor Atoms. *Can. J. chem.* **1975**, *53*, 177–182.
25. Jain, S.K.; Garg, B.S.; Bhoon, Y.K. Iron(III) complexes of 2-acetylpyridine-4-phenyl-3-thiosemicarbazones: Magnetic, E.s.r. and spectral studies. *Transit. Met. Chem.* **1986**, *11*, 89–95. [CrossRef]
26. Maurya, R.C.; Rajput, S. Neutral dioxovanadium(V) complexes of biomimetic hydrazones ONO donor ligands of bioinorganic and medicinal relevance: Synthesis via air oxidation of bis(acetylaceto-nato)oxovanadium(IV), characterization, biological activity and 3D molecular modeling. *J. Mol. Struct.* **2007**, *833*, 133–144. [CrossRef]
27. Sallam, S.A.; Orabi, A.S.; El-Shetary, B.A.; Lentz, A. Copper, nickel and cobalt complexes of Schiff-bases derived from β-diketones. *Transit. Met. Chem.* **2002**, *27*, 447–453. [CrossRef]
28. Tossidis, A.; Bolos, C.A. Monohalogenobenzoylhydrazones II. Synthesis and Study of Ti(IV) Complexes with Monochlorobenzoylhydrazones of 2-Furaldehyde, 2-Thiophenaldehyde, 2-Pyrrolaldehyde and Di-2-pyridylketone as Ligands. *Inorg. Chim. Acta* **1986**, *112*, 93–97. [CrossRef]
29. Ainscough, E.W.; Brodie, A.M.; Dobbs, A.J.; Ranford, J.D.; Waters, J.M. Antitumour copper(II) salicylaldehyde benzoylhydrazone (H_2sb) complexes: Physicochemical properties and the single-crystal X-ray structures of [{Cu(H_2sb)(CCl_3CO_2)$_2$}$_2$] and [{Cu(Hsb) (ClO_4) (C_2H_5OH)}$_2$] and the related salicylaldehyde acetylhydrazone (H_2sa) complex, [Cu(Hsa)Cl(H_2O)]·H_2O. *Inorg. Chim. Acta* **1998**, *267*, 27–38.
30. El-Sawaf, A.K.; Nassar, A.A.; El-Samanody, E. Synthesis, magnetic, spectral and biological studies of copper (II) complexes of 4-benzoyl-3-methyl-1-phenyl-2-pyrazolin-5-one N(4)-substituted thiosemicarbazones. *Sci. J. Chem.* **2014**, *2*, 17–26. [CrossRef]
31. Nair, M.K.M.; Radhakrishnan, P.K. Iodide Complexes of Yttrium and Lanthanides with 4-N-(4′-Antipyrylmethylidene) aminoantipyrine. *Synth. React. Inorg. Met. Org. Chem.* **1996**, *26*, 529–541. [CrossRef]
32. Afrasiabi, Z.; Sinn, E.; Padhye, S.; Dutta, S.; Padhye, S.; Newton, C.; Anson, C.E.; Powell, A.K. Transition metal complexes of phenanthrenequinone thiosemicarbazone as potential anticancer agents: Synthesis, structure, spectroscopy, electrochemistry and in vitro anticancer activity against human breast cancer cellline, T47D. *J. Inorg. Biochem.* **2003**, *95*, 306–314. [CrossRef]
33. Fouda, M.F.R.; Abd-Elzaher, M.M.; Shakdofa, M.M.; El-Saied, F.A.; Ayad, M.I.; el Tabl, A.S. Synthesis and Characterization of a Hydrazone Ligand Containing Antipyrine and its Transition Metal Complexes. *J. Coord. Chem.* **2008**, *61*, 1983–1996. [CrossRef]

34. Lever, A.B.P. Electronic Spectra of Some Transition Metal Complexes: Derivation of Dq and B. *J. Chem. Educ.* **1968**, *45*, 711–712. [CrossRef]
35. Shebl, M.; El-ghamry, M.A.; Khalil, S.M.; kishk, M.A. Mono- and binuclear copper(II) complexes of new hydrazone ligands derived from 4,6-diacetylresorcinol: Synthesis, spectral studies and antimicrobial activity. *Spectrochim. Acta A Mol. Biomol. Spectrosc.* **2014**, *21*, 232–241. [CrossRef] [PubMed]
36. Downes, J.M.; Whelan, J.; Bosnich, B. Biological analogs, Spectroscopic characteristics of mercapto- and disulfide-copper(II) coordination in relation to type I proteins. *Inorg. Chem.* **1981**, *20*, 1081–1086. [CrossRef]
37. Okawa, H.; Nakamoto, M.; Lzumitani, T.; Kida, S. Syntheses and Configurations of Copper(II) and Nickel(II) Complexes of *trans*-1,2-Dicyano-1,2-cyclohexanediamine. *Bull. Chem. Soc.* **1982**, *55*, 2671–2672. [CrossRef]
38. Suzuki, M.; Kanatomi, H.; Koyama, H.; Murase, I. Copper(I) and Copper(II) Complexes of Tripod Ligands, Tris(2-alkylthioethyl)amine. *Bull. Chem. Soc.* **1980**, *53*, 1961–1964. [CrossRef]
39. Kovala-Dermertzi, D.; Tsangaris, J.M.; Hadjiliadis, N. Complexes of aminobenzylamines. Part I. Complexes of *O*-aminobenzylamine with copper(II), cobalt(II) and nickel(II). *Transit. Met. Chem.* **1983**, *8*, 140–146. [CrossRef]
40. Suzuki, M.; Demura, H.K.Y.; Murase, I. Syntheses and Properties of Dinuclear Copper(II) Complexes with 2,6-Bis[bis(2-pyridylmethyl)aminomethyl]-4-methylphenol. *Bull. Chem. Soc.* **1984**, *57*, 1003–1007. [CrossRef]
41. El-Tabl, A.S.; El-Bahnasawy, R.M.; Hamdy, A.E.D. Synthesis, magnetic, spectral and antimicrobial studies on metal complexes of 4- methylphenylaminoacetoisatin hydrazine. *J. Chem. Res.* **2009**, *11*, 659–664.
42. Chohan, Z.H.; Pervez, H.; Khan, K.M.; Supuran, C.T. Metal binding and antibacterial activity of ciprofloxacin complexes. *J. Enzym. Inhib. Med. Chem.* **2005**, *20*, 303–307. [CrossRef] [PubMed]
43. Lever, A.B.P. *Inorganic Electronic Spectroscopy, Studies in Physical and Theoretical Chemistry*; Elsevier Science Ltd.: Amsterdam, The Netherlands, 1984.
44. Matovic, Z.D.; Miletic, V.D.; Samardzic, G.; Pelosi, G.; Ianelli, S.; Trifunovic, S. Square-planar copper(II) complexes with a tetradentate amido-carboxylate ligands. Crystal structure of Na_2[Cu(obap)]2·2H_2O. Strain analysis and spectral assignments of complexes. *Inorg. Chim. Acta* **2005**, *358*, 3135–3144. [CrossRef]
45. Mangalam, N.A.; Kurup, M.R.P. Versatile binding properties of a di-2-pyridyl ketone nicotinoylhydrazone ligand: Crystal structure of a Cu(II) complex. *Spectrochim. Acta Part A Mol. Biomol. Spectrosc.* **2011**, *78*, 926–934. [CrossRef] [PubMed]
46. Aly, M.M.; Imam, S.M. Characterization of Copper(II), nickel(II), cobalt(II) and palladium(II) complexes of vicinal oxime-imine ligands; induced chelate isomerism in the same molecule of the nickel(II) complex. *Mon. Chem. Chem. Mon.* **1995**, *126*, 173–185. [CrossRef]
47. el Saied, F.A.; Shakdofa, M.M.E.; el Tabl, A.S.; Elzaher, M.M.A. Coordination behaviour of N′1,N′4-bis((1, 5-dimethyl-3-oxo-2-phenyl-2,3-dihydro-1H-pyrazol-4-yl)methylene) succinohydrazide toward transition metal ions and their antimicrobial activities. *Main Group Chem.* **2014**, *13*, 87–99.
48. Pahonțu, E.; Ilieș, D.C.; Shova, S.; Oprean, C.; Păunescu, V.; Olaru, O.T.; Rădulescu, F.Ș.; Gulea, A.; Roșu, T.; Drăgănescu, D. Synthesis, Characterization, Antimicrobial and Antiproliferative Activity Evaluation of Cu(II), Co(II), Zn(II), Ni(II) and Pt(II) Complexes with Isoniazid-Derived Compound. *Molecules* **2017**, *22*, 650.
49. Earnshaw, A. *Introduction to Magneto-Chemistry*; Academic Press: New York, NY, USA, 1968.
50. Chandra, S.; Sharma, K.K. Cobalt(II) and nickel(II) complexes of some nitrogen-oxygen and nitrogen-sulphur ligands. *Transit. Met. Chem.* **1984**, *9*, 1–3. [CrossRef]
51. El-Tabl, A.S.; El-Saied, F.A.; Al-Hakimi, A.N. Synthesis, spectroscopic investigation and biological activity of metal complexes with ONO trifunctionalalized hydrazone ligand. *Transit. Met. Chem.* **2007**, *32*, 689–701. [CrossRef]
52. Fouda, M.F.R.; Abd-El-zaher, M.M.; Shakdofa, M.M.; El-Saied, F.A.; Ayad, M.I.; El-Tabl, A.S. Synthesis and characterization of transition metal complexes of *N*′-[(1, 5-dimethyl-3-oxo-2-phenyl-2, 3-dihydro-1H-pyrazol-4-yl) methylene] thiophene-2-carbohydrazide. *Transit. Met. Chem.* **2008**, *33*, 219–228. [CrossRef]
53. Al-Tabl, A.S.; AbouEl-Enein, S.A. Reactivity of the new potentially binucleating ligand, 2-(acetichydrazido-*N*-methylidene-α-naphthol)-benzothiazol, towards manganese (II), nickel (II), cobalt (II), copper (II) and zinc (II) salts. *J. Coord. Chem* **2004**, *57*, 281–294. [CrossRef]
54. El-Reash, G.M.A.; Ibrahim, K.M.; Bekheit, M.M. Structural studies of 4(phenyl or benzamidos)-1-cyclohexanone-3- thiosemicarbazone complexes. *Transit. Met. Chem.* **1990**, *15*, 148–151.

55. El-Saied, F.A.; El-Asmy, A.A.; Kaminsky, W.; West, D.X. Spectral and structural studies of cobalt(II,III), nickel(II), and copper(II) complexes of dehydroacetic acid *N*4-dialkyl- and 3-azacyclothiosemicarbazones. *Transit. Met. Chem.* **2003**, *28*, 954–960. [CrossRef]
56. El-Tabl, A.S.; Shakdofa, M.M.E.; El-Seidy, A.M.A.; Al-Hakimi, A.N. Synthesis, characterization and antifungal activity of metal complexes of 2-(5-((2-chlorophenyl) diazenyl)-2-hydroxybenzylidene) hydrazinecarbothioamide. *Phosphorus Sulfur Silicon Relat. Elem.* **2012**, *187*, 1312–1323. [CrossRef]
57. Kasumov, V.T.; Köksal, F. Synthesis, ESR, UV-Visible and reactivity studies of new bis(*N*-dimethoxyaniline-3,5-(t)Bu2-salicylaldiminato)copper(II) complexes. *Spectrochim. Acta A Mol. Biomol. Spectrosc.* **2012**, *98*, 207–214. [CrossRef] [PubMed]
58. Hathaway, B.J.; Billing, D.E. The electronic properties and stereochemistry of mono-nuclear complexes of the copper(II) ion. *Coord. Chem. Rev.* **1970**, *5*, 1949. [CrossRef]
59. Zaky, R.R.; Ibrahim, K.M.; Gabr, I.M. Bivalent transition metal complexes of o-hydroxyacetophenone [*N*-(3-hydroxy-2-naphthoyl)] hydrazone: Spectroscopic, antibacterial, antifungal activity and thermogravimetric studies. *Spectrochim. Acta A Mol. Biomol. Spectrosc.* **2011**, *81*, 28–34. [CrossRef] [PubMed]
60. Brown, D.R.; West, D.X. An ESR study of addition species formed between bis(2-thiopyridine N-oxide)Cu(II) and heterocyclic and aliphatic amines. *J. Inorg. Nucl. Chem.* **1981**, *43*, 1017–1021. [CrossRef]
61. Nagashri, K.; Joseph, J.; Dhanaraj, C.J. Copper (II) complexes of hydroxyflavone derivatives as potential bioactive molecule to combat antioxidants: Synthesis, characterization and pharmacological activities. *Appl. Organomet. Chem.* **2011**, *25*, 704–717. [CrossRef]
62. Proctor, I.M.; Hathaway, B.J.; Nicholis, P. The electronic properties and stereochemistry of the copper(II) ion. Part I. Bis(ethylenediamine)copper(II) complexes. *J. Chem. Soc. A* **1968**, 1678–1684. [CrossRef]
63. Kivelson, D.; Neiman, R. ESR Studies on the Bonding in Copper Complexes. *J. Chem. Phys.* **2004**, *35*, 149. [CrossRef]
64. Shauib, N.M.; Elassar, A.Z.A.; El-Dissouky, A. Synthesis and spectroscopic characterization of copper(II) complexes with the polydentate chelating ligand 4,4′-[1,4-phenylenedi(nitrilo)dipente-2-one. *Spectrochim. Acta Part A Mol. Biomol. Spectrosc.* **2006**, *63*, 714–722. [CrossRef] [PubMed]
65. Ray, R.K.; Kauffmann, G.B. An EPR study of copper(II)-substituted biguanide complexes. Part III. *Inorg. Chim. Acta* **1990**, *174*, 237–244. [CrossRef]
66. Hathaway, B.J. A new look at the stereochemistry and electronic properties of complexes of the copper(II) ion. *Complex Chem.* **1984**, *57*, 55–118.
67. Sakaguchi, U.; Adison, A.W. Spectroscopic and redox studies of some copper(II) complexes with biomimetic donor atoms: Implications for protein copper centres. *J. Chem. Soc. Dalton Trans.* **1979**, *4*, 600–608. [CrossRef]
68. El-Tabl, A.S. Synthesis and spectral studies on mononuclear copper (II) complexes of isonitrosoacetylacetone ligand. *Polish J. Chem.* **1997**, *71*, 1213–1222.
69. Mahajian, M.; Saxena, K.N.; Saxen, P.C. ESR study of Cu(II) complexes. *Inorg. Nucl.Chem.* **1981**, *43*, 2148–2149. [CrossRef]
70. Oscar, C. Biopharmacological studies on certain new anticancer drugs. *J. Biochem.* **1988**, *110*, 701–707.
71. Tagmizyan, W.A. Metabolism of impaired glucose in patients with neoplasia. *Am. Biol.* **1990**, *2*, 53–58.
72. Silverstein, H.; Dervot, K.; Oscar, D. Studies on carbohydrate metabolism and different types of tumors bearing animals. *Lancet* **1988**, *22*, 40–45.
73. Kind, P.R.N.; Gordon, M.; Laverick, M.; Nias, A.H.; Slavin, B.M. The effect of C3H mouse mammary tumor on the levels of serum and urine analytes in vivo. *Br. J. Cancer* **1985**, *52*, 607–612. [CrossRef] [PubMed]
74. Parveen, A.; Subedi, L.; Kim, H.W.; Khan, Z.; Zahra, Z.; Farooqi, M.Q.; Kim, S.Y. Phytochemicals Targeting VEGF and VEGF-Related Multifactors as Anticancer Therapy. *J. Clin. Med.* **2019**, *8*, 350. [CrossRef] [PubMed]
75. Abd-Alhaseeb, M.M.; Zaitone, S.A.; Abou-El-Ela, S.H.; Moustafa, Y.M. Olmesartan Potentiates the Anti-Angiogenic Effect of Sorafenib in Mice Bearing Ehrlich's Ascites Carcinoma: Role of Angiotensin (1–7). *PLoS ONE* **2014**, *9*, e85891. [CrossRef] [PubMed]
76. Liang, Y.; Brekken, R.A.; Hyder, S.M. Vascular endothelial growth factor induces proliferation of breast cancer cells and inhibits the anti-proliferative activity of anti-hormones. *Endocr. Relat. Cancer* **2006**, *13*, 905–919. [CrossRef] [PubMed]
77. Kumar, S.; Cieplak, P. Effect of phosphorylation and single nucleotide polymorphisms on caspase substrates processing. *Apoptosis* **2018**, *23*, 194–200. [CrossRef] [PubMed]

78. Hassan, M.; Watari, H.; AbuAlmaaty, A.; Ohba, Y.; Sakuragi, N. Apoptosis and Molecular Targeting Therapy in Cancer. *BioMed Res. Int.* **2014**, *2014*, 150845. [CrossRef] [PubMed]
79. Cao, Z.; Yang, Q.; Yin, H.; Qi, Q.; Li, H.; Sun, G.; Wang, H.; Liu, W.; Li, J. Peroxynitrite induces apoptosis of mouse cochlear hair cells via a Caspase-independent pathway in vitro. *Apoptosis* **2017**, *22*, 1419–1430. [CrossRef] [PubMed]
80. Vance, N.R.; Gakhar, L.; Spies, M.A. Allosteric Tuning of Caspase-7: A Fragment-Based Drug Discovery Approach. *Angew. Chem. Int. Ed. Engl.* **2017**, *56*, 14443–14447. [CrossRef] [PubMed]
81. Zahran, M.A.-H.; El-Aarag, B.; Mehany, A.B.M.; Belal, A.; Younes, A.S. Design, synthesis, biological evaluations, molecular docking, and in vivo studies of novel phthalimide analogs. *Arch. Pharm. Chem. Life Sci.* **2018**, *351*, 1–12. [CrossRef] [PubMed]
82. Salem, M.L.; Shoukry, N.M.; Teleb, W.K.; Abdel-Daim, M.M.; Abdel-Rahman, M.A. In vitro and in vivo antitumor effects of the Egyptian scorpion Androctonus amoreuxi venom in an Ehrlich ascites tumor model. *SpringerPlus* **2016**, *5*, 570. [CrossRef]
83. Marcelli, M.; Cunningham, G.R.; Walkup, M.; He, Z.; Sturgis, L.; Kagan, C.; Mannucci, R.; Nicoletti, I.; Teng, B.; Denner, L. Signaling Pathway Activated during Apoptosis of the Prostate Cancer Cell Line LNCaP: Overexpression of Caspase-7 as a New Gene Therapy Strategy for Prostate Cancer. *Cancer Res.* **1999**, *59*, 382–390. [PubMed]
84. Guirgis, A.A.; Zahran, M.; Mohamed, A.S.; Talaat, R.M.; Abdou, B.Y.; Agwa, H.S. Effect of thalidomide dithiocarbamate analogs on the intercellular adhesion molecule-1 expression. *Int. Immunopharmacol.* **2010**, *10*, 805–811. [CrossRef] [PubMed]
85. Zahra, M.H.; Salem, T.A.; El-Aarag, B.; Yosri, N.; EL-Ghlban, S.; Zaki, K.; Marei, A.H.; Abd El-Wahed, A.; Saeed, A.; Khatib, A.; et al. *Alpinia zerumbet* (Pers.): Food and Medicinal Plant with Potential In Vitro and In Vivo Anti-Cancer Activities. *Molecules* **2019**, *24*, 2495. [CrossRef] [PubMed]
86. Papadopoulos, D.; Kimler, B.F.; Estes, N.C.; Durham, F.J. Growth delay effect of combined interstitial hyperthermia and brachytherapy in a rat solid tumor model. *Anticancer Res.* **1989**, *9*, 45–47. [PubMed]
87. El-Aarag, B.; Hussein, W.; Ibrahim, W.; Zahran, M. Thymoquinone Improves Anti-Diabetic Activity of Metformin in Streptozotocin-Induced Diabetic Male Rats. *J. Diabetes Metab.* **2017**, *8*, 780.
88. Chen, J.; Stavro, P.M.; Thompson, L.U. Dietary Flaxseed Inhibits Human Breast Cancer Growth and Metastasis and Downregulates Expression of Insulin-Like Growth Factor and Epidermal Growth Factor Receptor. *Nutr. Cancer* **2002**, *43*, 187–192. [CrossRef] [PubMed]

Sample Availability: Samples of the compounds are available from the authors.

© 2019 by the authors. Licensee MDPI, Basel, Switzerland. This article is an open access article distributed under the terms and conditions of the Creative Commons Attribution (CC BY) license (http://creativecommons.org/licenses/by/4.0/).